Searching for calorons and dyons in SU(3) gluodynamics near the transition and in deconfinement

E.-M. Ilgenfritz

VBLHEP and BLTP, Joint Institute for Nuclear Research, Dubna, Russia

Collaborators:

V. G. Bornyakov

B. V. Martemyanov

ITEP Moscow, Russia

M. Müller-Preussker

Humboldt-Universität Berlin, Germany

XI-th Quark Confinement and the Hadron Spectrum

St. Petersburg, Russia, September 8–12, 2014

Since Confinement X (2012 in Munich) we have lost two colleagues and friends which have fundamentally contributed to the subject of the particular topological structure of QCD that we are visualizing and investigating numerically on the lattice. We enjoyed collaboration, correspondence and many discussions.

Dmitri Igorevich Diakonov, PNI, St. Petersburg

* 30. 3. 1949 † 26. 12. 2012

Pierre van Baal, University Leiden

* 9. 6. 1955 † 29. 12. 2013

I am are also sadly missing the founder of the Lattice Gauge Theory community in Russia, friend and collaborator, and close ally in various scientific and scientific-political aspects.

Mikhail Igorevich Polikarpov, ITEP Moscow

* 28. 12. 1952 † 18. 7. 2013

Our current work is dedicated to the memory of these colleagues.

Outline of the talk

Central for our work are the Kraan/van Baal/Lee/Lu caloron, (with non-trivial holonomy in the confinement phase), its constituents, N_c dyons and N_c antidyons, and their manifestation in the Dirac spectrum. Moreover, ...

they are the basic degrees of freedom in the confinement model of Diakonov and Petrov (V. Petrov, Monday, parallel 1, A1)

1. Introduction and some history
2. Briefly about calorons and dyons
3. Dyons in SU(3) below the transition and slightly above
4. The dyonic picture deeper in deconfinement
5. Summary and outlook

I. Introduction and some history

Chronology

- Our starting point was the attempt ro reach a semiclassical-style simulation of both confinement and chiral symmetry breaking, based on a description of the vacuum at the infrared scale of 0.3 to 0.4 fm, similar to Shuryak's and T. Schaefer's instanton simulations.
- This goal cannot be achieved within the classical instanton picture. Dmitri Diakonov had ideas about improving that, too.
- The discovery of Kraan-van-Baal-Lee-Lu caloron gave hope, to contribute to the understanding of confinement as well as for chiral symmetry breaking, by means of the "dissolution" of instantons (Kraan and van Baal, 1998) into instanton quarks. The dependence of the solutions on the "external" holonomy turned out to be an additional virtue.

- Diakonov, Gromov, Petrov and Silovskiy (2004) calculated the analog of t'Hooft's instanton amplitude, the weight for $SU(2)$ calorons with non-trivial holonomy.
- Simulation of $SU(2)$ caloron gases was qualitatively successful to explain confinement of fundamental quarks, but not quantitatively (Gerhold, E.-M. I, Müller-Preussker, hep-ph/0607315). Details of the distribution of the caloron parameters remained poorly understood.
- The existence of center vortices in caloron fields and their possible contribution to confinement by caloron gases was demonstrated next (Bruckmann, E.-M.I., Martemyanov, Bo Zhang, arXiv:0912.4186).

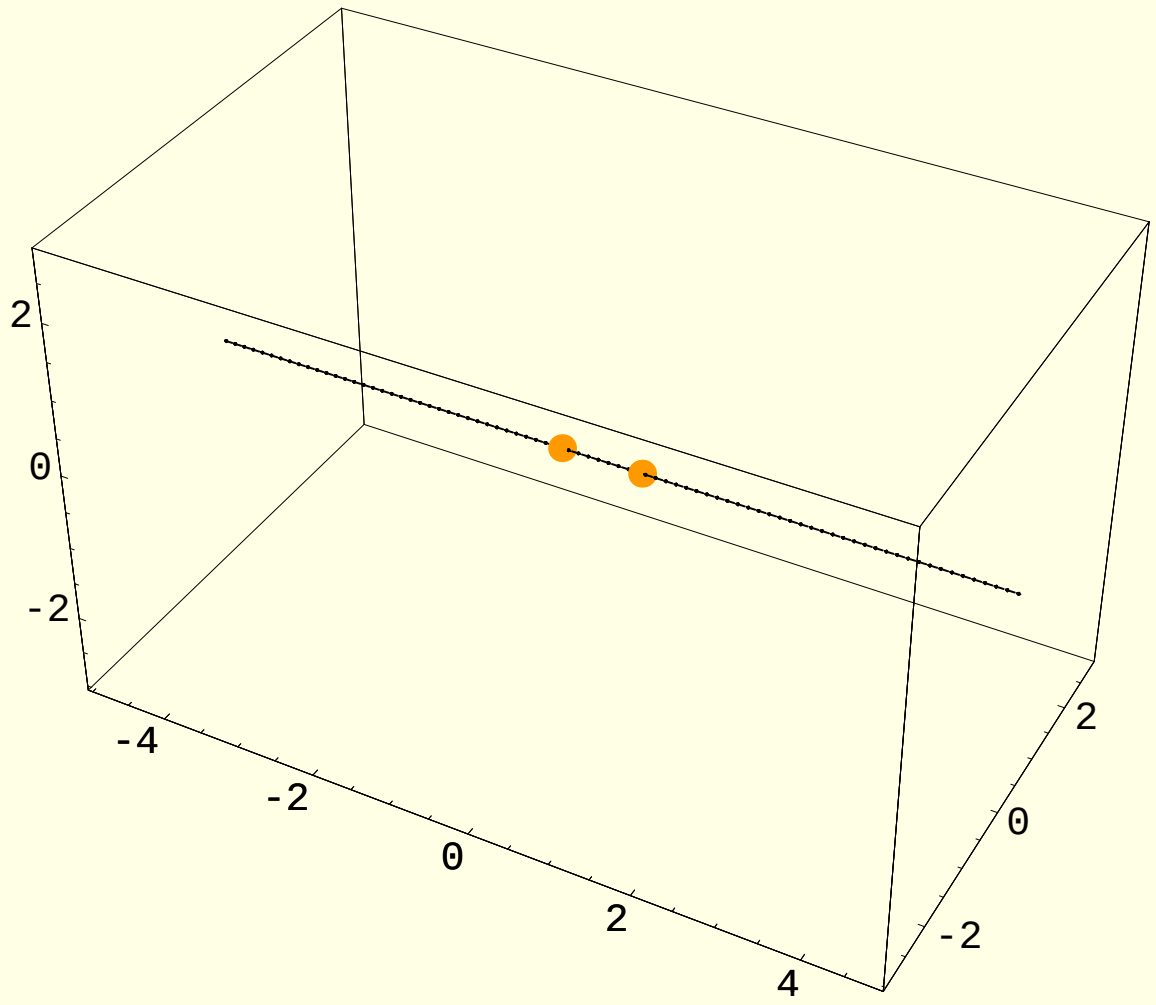

Figure 1: The dyon charge induced part of the vortex from the singlet first excited mode (performing the Laplacian center gauge) as measured in a caloron with holonomy $\varnothing = 0.25$ and $\rho = 0.6\beta$ in a time slice. The outcome is identical to the x_3-axis and the same for all time slicesi (static vortex plane). The dots denote points on the vortex (lines along x_0) where the flux changes, i.e. the location of LAG-monopoles.

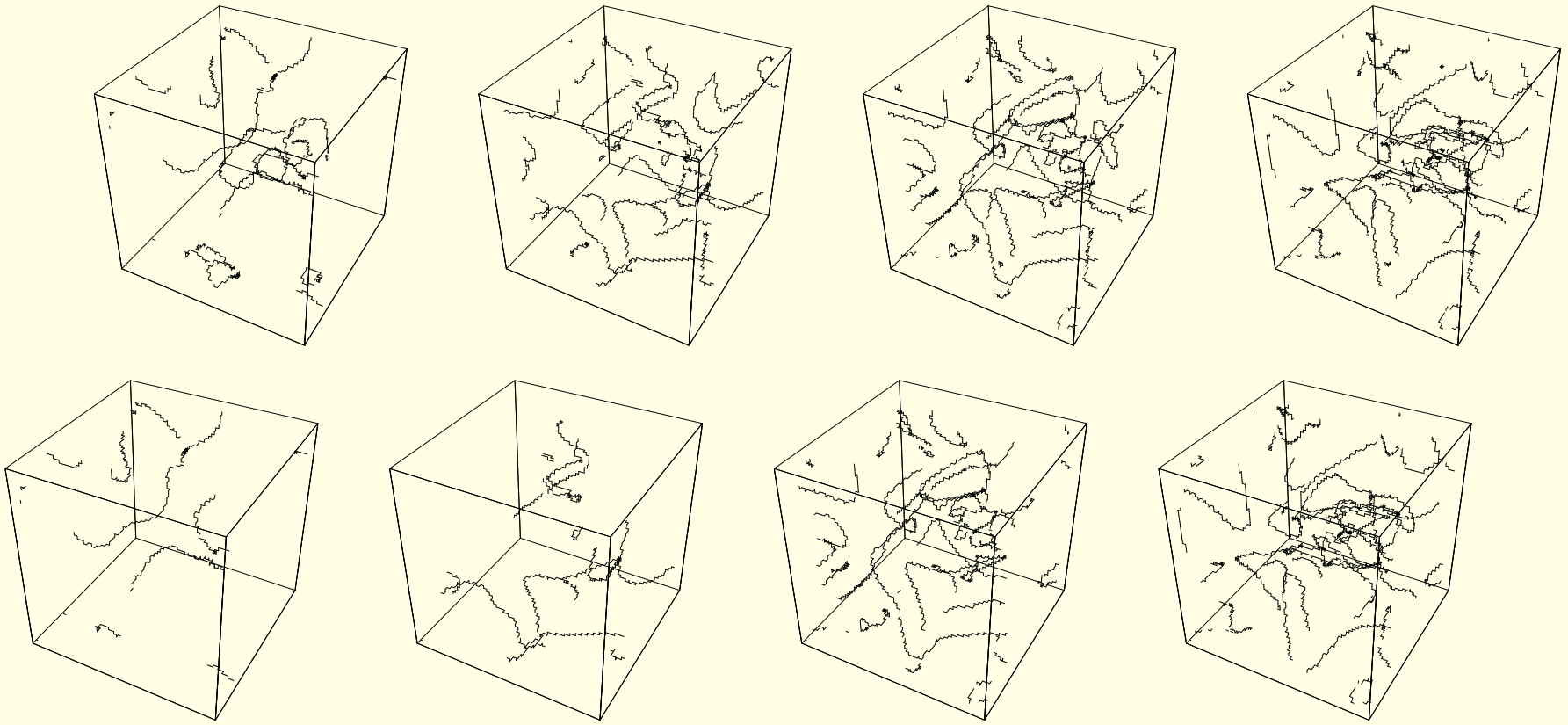

Figure 2: The space-time part of vortices in caloron ensembles in a fixed time slice. The asymptotic Polyakov loop varies from left to right: $\omega = \{0.0625, 0.0125, 0.01875, 0.25\}$ (from deconfined phase to confined phase). The upper row shows the entire vortex content in each caloron ensemble, the lower row shows the corresponding biggest vortex cluster.

- In 2008, Diakonov and Petrov stepped forward to "Statistical physics of dyons and quark confinement" (with only dyons or antidyons !) which could be solved in closed form in a field-theoretic way with qualitatively correct results:

$$\sigma = (8\ \rho\ T)^{1/2} \qquad T_{\text{dec}} = \left(48\ \rho\ T/\pi^2\right)^{1/4} \text{ for SU(2)}$$

$$\frac{T_{\text{dec}}}{\sqrt{\sigma}} = \left(\frac{6}{\pi^2}\right)^{1/4}$$

ρT is the four-dimensional dyon (not instanton !) density.

- The moduli space metric for arbitrary numbers m_i of dyons of type $i = 1, \ldots, N_c$ (obtained by analogy from the $SU(2)$ $Q_t = 1$ caloron by Diakonov and Petrov) turned out to pose a sign problem preventing us (up to now) from the simulation of dyon systems (Bruckmann, Dinter, E.-M. I., Müller-Preussker, Wagner, arXiv:0903.3075) with this measure.

- Two pragmatic ways out, a dyon system with two-body interactions (dealt with by HMC) and without interactions (by sampling of a random dyon gas), have been studied as representing the confinement phase with interesting results.

  The non-interacting case has an analytic solution $\sigma = \frac{\pi}{2}\frac{\rho}{T}$.

  To reproduce this by random sampling (the extrapolation from a finite to ∞ sampling volume) has required the application of Ewald summation techniques (Bruckmann, Dinter, E.-M.I., Müller-Preussker, Wagner, Maier, arXiv:1111.3158, also PoS ConfinementX (2012) 051, arXiv:1212.5557).

  This method (apparently less known to particle physicists) might be useful in many similar problems.

Simulating with the two-body factorized, positive weight, compared with the non-interacting case (random sampling)

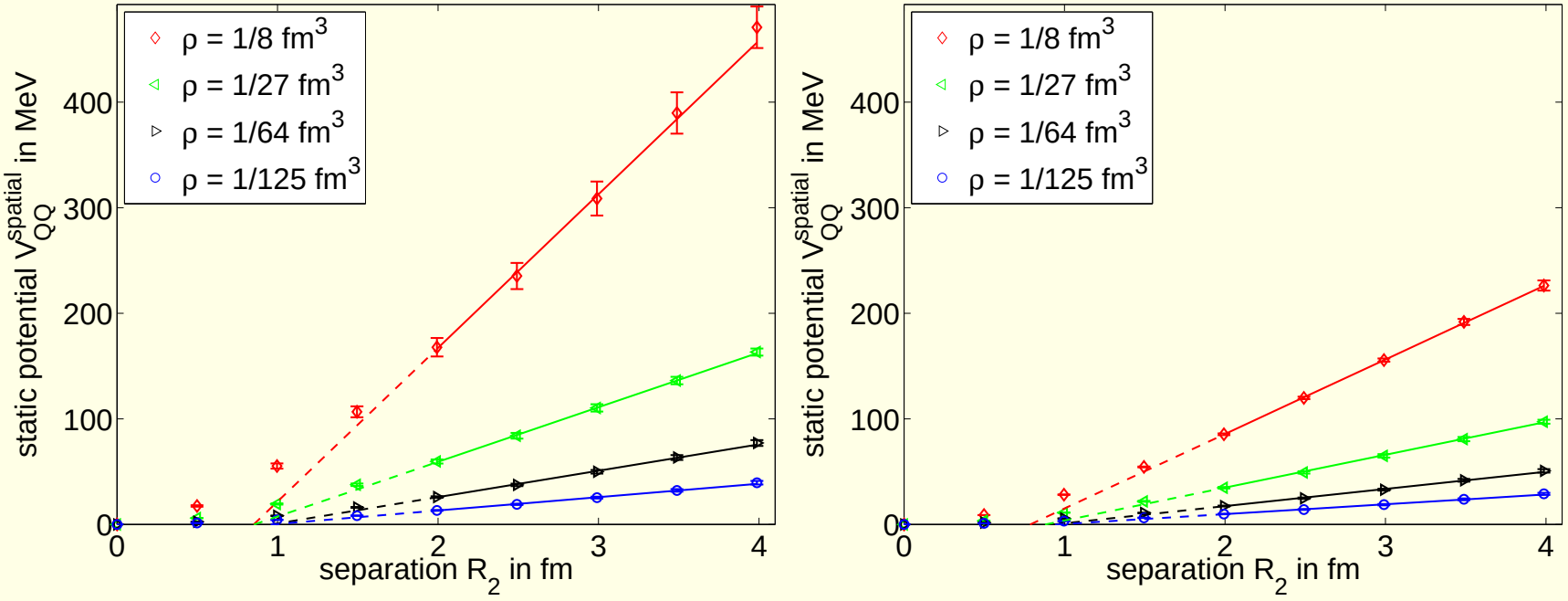

Figure 3: Static potentials $V_{Q\bar{Q}}^{\text{spat}}$ from spatial Wilson loops for sampling without interaction (left) and for Metropolis simulation of the two-body factorized measure.

The slope of the non-interacting system is steeper at high density and flatter at low density compared with the two-body interacting system.

Pair distribution of same and different dyon kind: screening

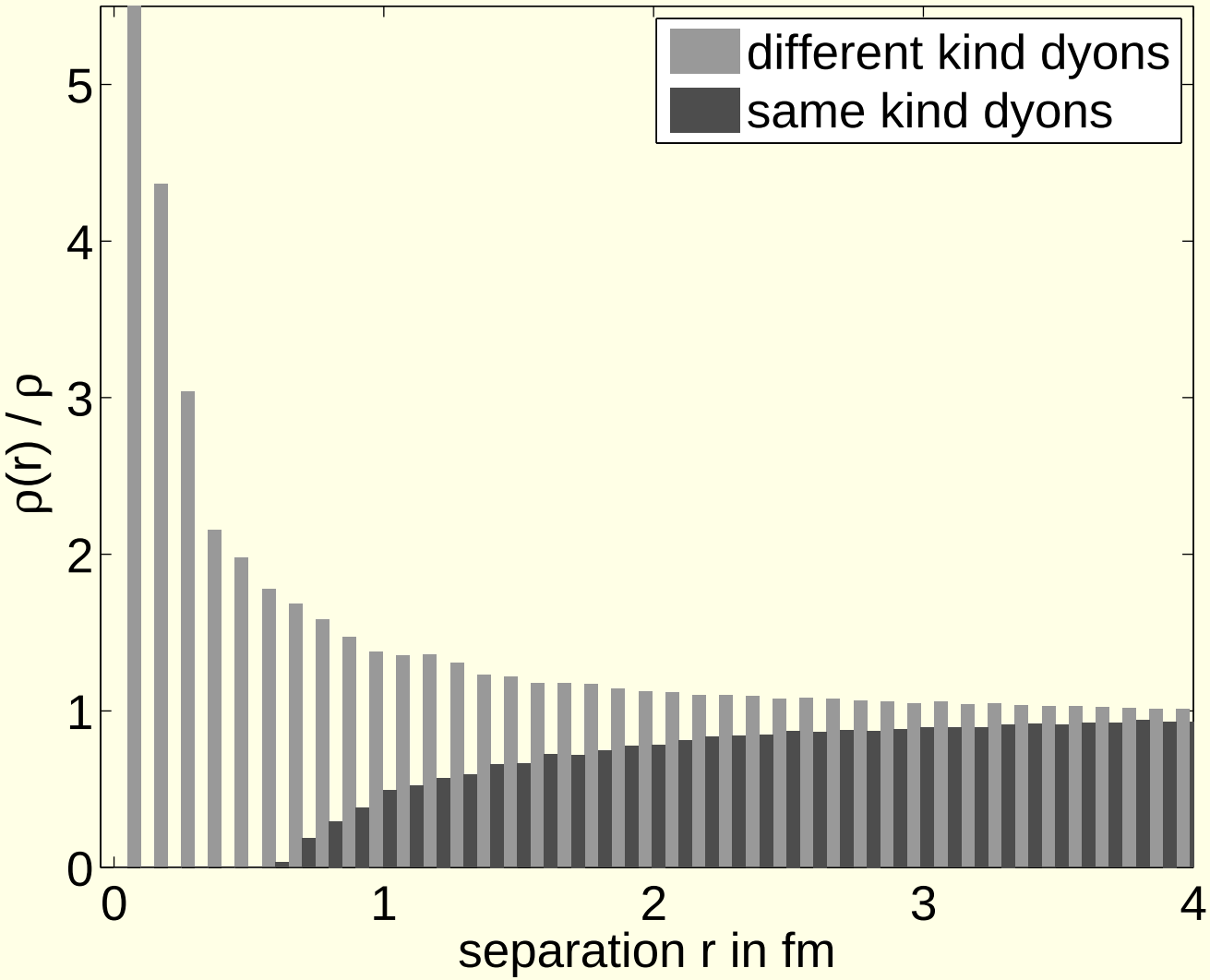

Figure 4: Pair distribution for same and different kind of dyons in a system of $n_D = 200$ dyons with a density $\rho = 1/125\text{fm}^3$.

The $Q\bar{Q}$ free energy from the Polyakov loop correlator

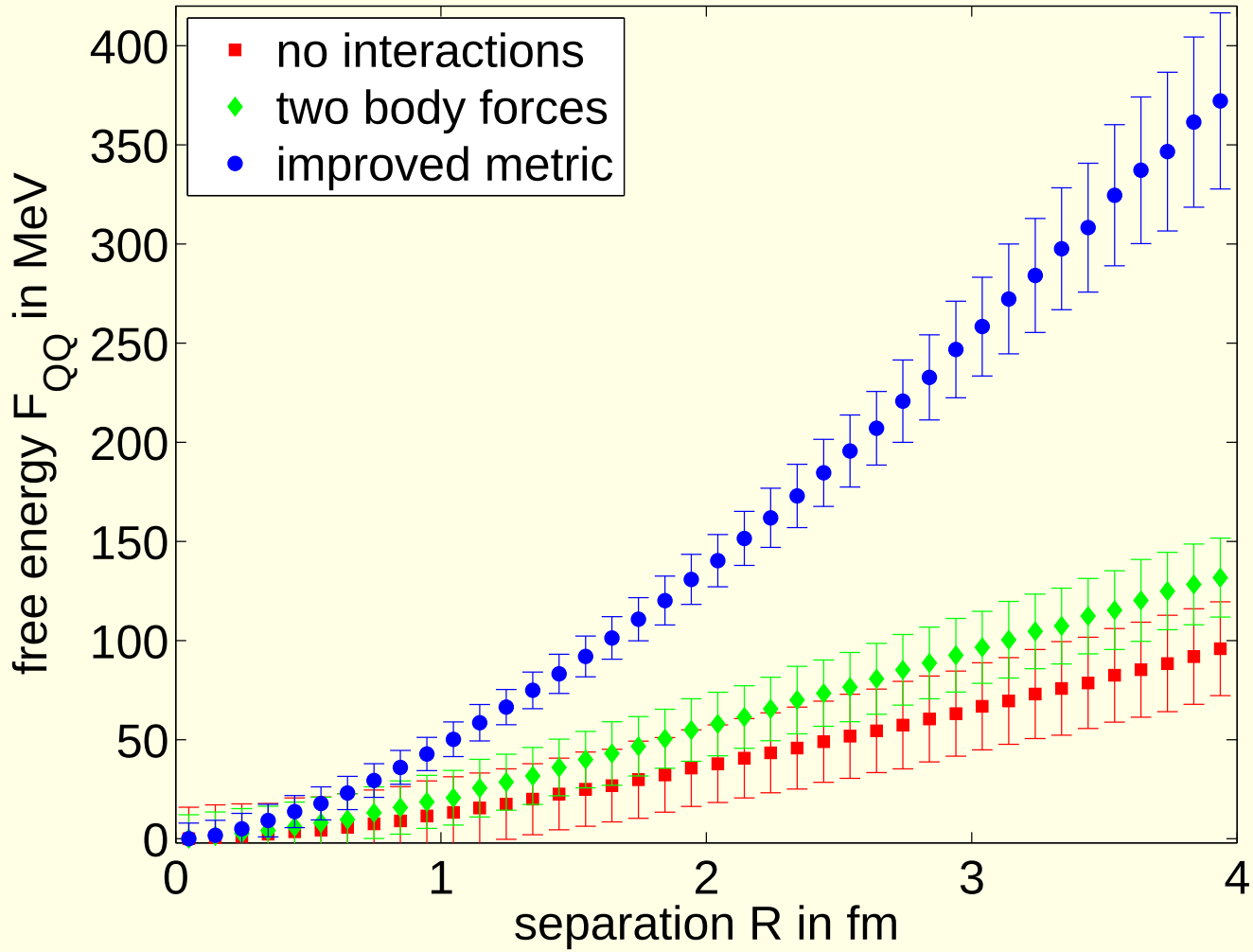

Figure 5: The free energy from the Polyakov loop correlator including $n_D = 200$ dyons for random sampling, for the two-body factorized weight and for the HMC simulation of the full measure $\det G$. All curves are for a density $\rho = 1/125\text{fm}^3$.

- For the discovery of dyon-like structures in physical lattice ensembles the use of overlap fermions turned out to be advantageous.

  This technique has been applied in the years 2007–2009 to $SU(2)$ Yang-Mills theory at the thermal phase transition and in deconfinement (Bornyakov, E.-M.I., Martemyanov, Morozov, Müller-Preussker and Veselov).
  (arXiv: 0706.4206, 0807.1980, 0809.2142)

  The interplay between Polyakov loop and topology has been semi-quantitatively discussed for $SU(2)$ gauge theory in

  F. Bruckmann, arXiv: 0901.0987 "How instantons survive ..."
  Confinement 8, 2008

- Recently (2013/2014) : the overlap fermionic method of dyon search was extended to $SU(3)$ with new features:

  three types of dyons, complex patterns of the Polyakov loop.
  (Bornyakov, E.-M.I., Martemyanov, Müller-Preussker)

  1. Analysis of low lying modes of the overlap Dirac operator: $T \approx T_c$

     Topology near the transition temperature in lattice gluodynamics analyzed by low lying modes of the overlap Dirac operator,

     E.-M.I., B.V. Martemyanov, M. Müller-Preussker

     Phys. Rev. D89:054503 (2014) [arXiv: 1309.7850 [hep-lat]]

  2. Analysis of low lying modes of the overlap Dirac operator: $T > T_c$

     Infrared topological structures in the deconfining phase of SU(3) gluodynamics: a unified view on low lying Dirac modes, topological clusters and Abelian monopoles

     V.G. Bornyakov, E.-M.I., B.V. Martemyanov, M. Müller-Preussker

     in preparation

Two lattice-empirical origins of inspiration for our work:

1. Close relation between chiral symmetry breaking/restoration and confinement/deconfinement pointed out by Ch. Gattringer, F. Bruckmann et al. 2006/2008
   - The Dirac spectrum becomes sensitive on the change of temporal boundary conditions above T_{dec}.
   - This signals the high temperature phase (vanishing chiral condensate, a non-vanishing Polyakov loop).
   - Question: Why does the spectrum change above T_c with the change of boundary conditions ?
   - Question: How does the nature of the lowest modes change: localization etc. ?

2. Stephanov's generalization of findings by S. Chandrasekharan, N. Christ et al., concluding that in $SU(3)$ gauge theory above T_c in the sector of the Polyakov loop $\langle L \rangle =$ acomplex the chiral symmetry is restored at a higher T than in the sector $\langle L \rangle =$ real . Phys. Lett. B375:249 (1996) [arXiv: hep-lat/9601001]

   - Similarly in $SU(2)$ gauge theory, in the sector of $\langle L \rangle < 0$ the chiral condensate would stay nonzero for all T.
   - For $SU(3)$ this was disproved by Ch. Gattringer et al., Phys. Rev. D66:054502 (2002) [arXiv:hep-lat/0202009]
   - The status for $SU(2)$ was clarified in our work Phys. Rev. D76:054505 (2007) [arXiv:0706.4206 [hep-lat]] The prediction is confirmed.
   - Question: Is the Polyakov loop the reason for opening a gap or not ? How does the mechanism of chiral symmetry restoration depend on the holonomy ? What is then different for $SU(3)$ compared to $SU(2)$?

II. Briefly about calorons and dyons

1. Generalities on $SU(N)$ calorons (following van Baal)

   Simple formula for a charge-one $SU(N)$ caloron action density ($= \pm$ topological density) derived from a potential ψ:

$$\text{Tr } F^2_{\alpha\beta}(x) = \partial^2_\alpha \partial^2_\beta \log \psi(x), \quad \psi(x) = \frac{1}{2}\text{tr}(\mathcal{A}_N \cdots \mathcal{A}_1) - \cos(2\pi t)\,.$$

   With index $m = 1, ..., N$ numbering the constituents, the 2×2 matrices are

$$\mathcal{A}_m = \frac{1}{r_m} \begin{pmatrix} r_m & |\vec{\rho}_{m+1}| \\ 0 & r_{m+1} \end{pmatrix} \begin{pmatrix} \cosh(2\pi\nu_m r_m) & \sinh(2\pi\nu_m r_m) \\ \sinh(2\pi\nu_m r_m) & \cosh(2\pi\nu_m r_m) \end{pmatrix},$$

   expressed through the distances from/between centers $\vec{y}_i$

$$r_m = |\vec{x} - \vec{y}_m|, \quad \vec{\rho}_m = \vec{y}_m - \vec{y}_{m-1}$$

   setting $b = 1/T = 1$ as length scale.

Parameters :

positions (approximately those of constituent monopoles) :

$$\vec{y}_1,\ \vec{y}_2, ..., \vec{y}_N$$

asymptotic holonomy (untraced Polyakov loop) :

$$\mathcal{P}_\infty = \text{diag}\left(e^{2\pi i \mu_m}\right), \quad \sum_{m=1}^{N} \mu_m = 0$$

with eigenphases, ordered as

$$\mu_1 < \mu_2 < .. < \mu_N < \mu_{N+1} \equiv 1 + \mu_1\,,$$

determining how action (and topological charge) is fractionally distributed among the lumps:

$$S_m = \nu_m\ S_{inst} \quad \text{with} \quad \nu_m = \mu_m - \mu_{m-1}\,.$$

Fermion zero-mode (present according to index theorem), can be endowed with a periodicity to be varied at will :

$$\Psi_z(t + 1/T, \vec{x}) = e^{-2\pi i z}\ \Psi_z(t, \vec{x})\,.$$

Jumping and delocalization (breathing) of zero-mode:

for $z \in [\mu_m, \mu_{m+1}]$ $\Rightarrow$ $|\Psi_z(x)|^2$ localized at $\vec{y}_m$

if $z \to \mu_m$ $\Rightarrow$ $|\Psi_z(x)|^2$ becomes delocalized

A specific feature of Neuberger overlap fermions:

- Zero modes are clearly identified, with chirality $= \pm 1$
- The index theorem is trivially fulfilled: $N_{\mathrm{zm}} = |Q_t|$
- Further (paired) topological objects must give rise to pairs of near-zero modes ($N_{\mathrm{nzm}} \neq 0$) that become clearly separable at $T > T_c$ (see later).

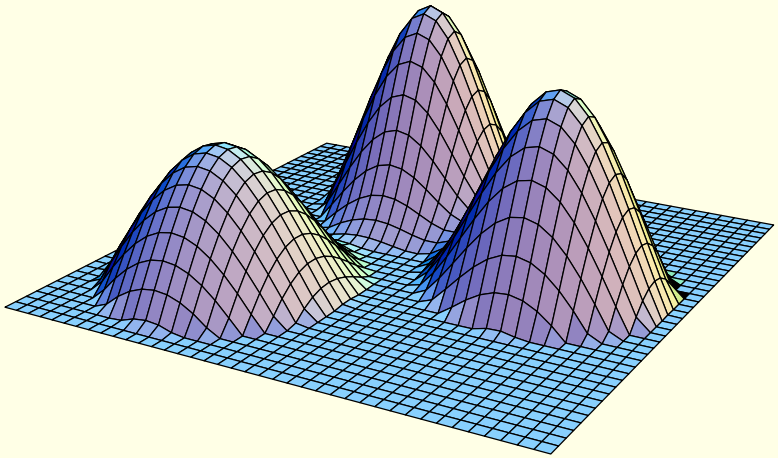

Figure 6: Logarithmic plot of the action density of a $SU(3)$ caloron with non-maximal non-trivial holonomy

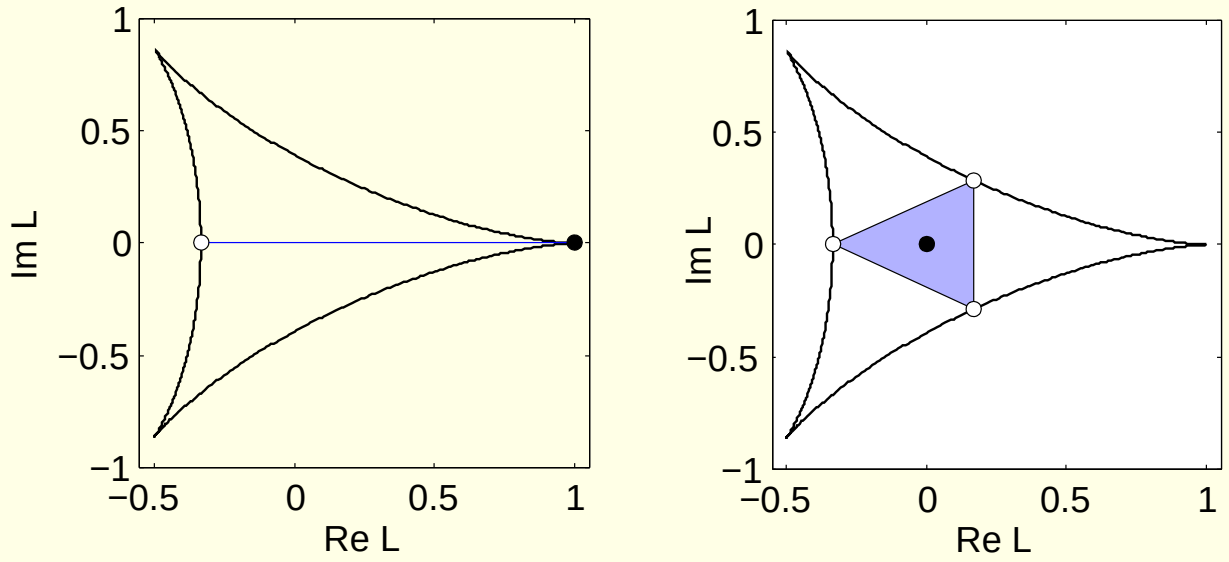

Figure 7: Schematic scatterplots in the complex plane (left: on the real axis, right: inside the triangle) of the local Polyakov loop values $L(\vec{x})$, for a caloron with trivial holonomy $L_\infty = +1$ (left) and with maximally non-trivial holonomy $L_\infty = 0$ (right). Black dots indicate the asymptotic Polyakov loop values, whereas white circles on the boundary give the local Polyakov loop values at the monopole constituents according to two eigenvalues of $\mathcal{P}$ becoming degenerate.

$SU(2)$: A small caloron: action density and Polyakov loop

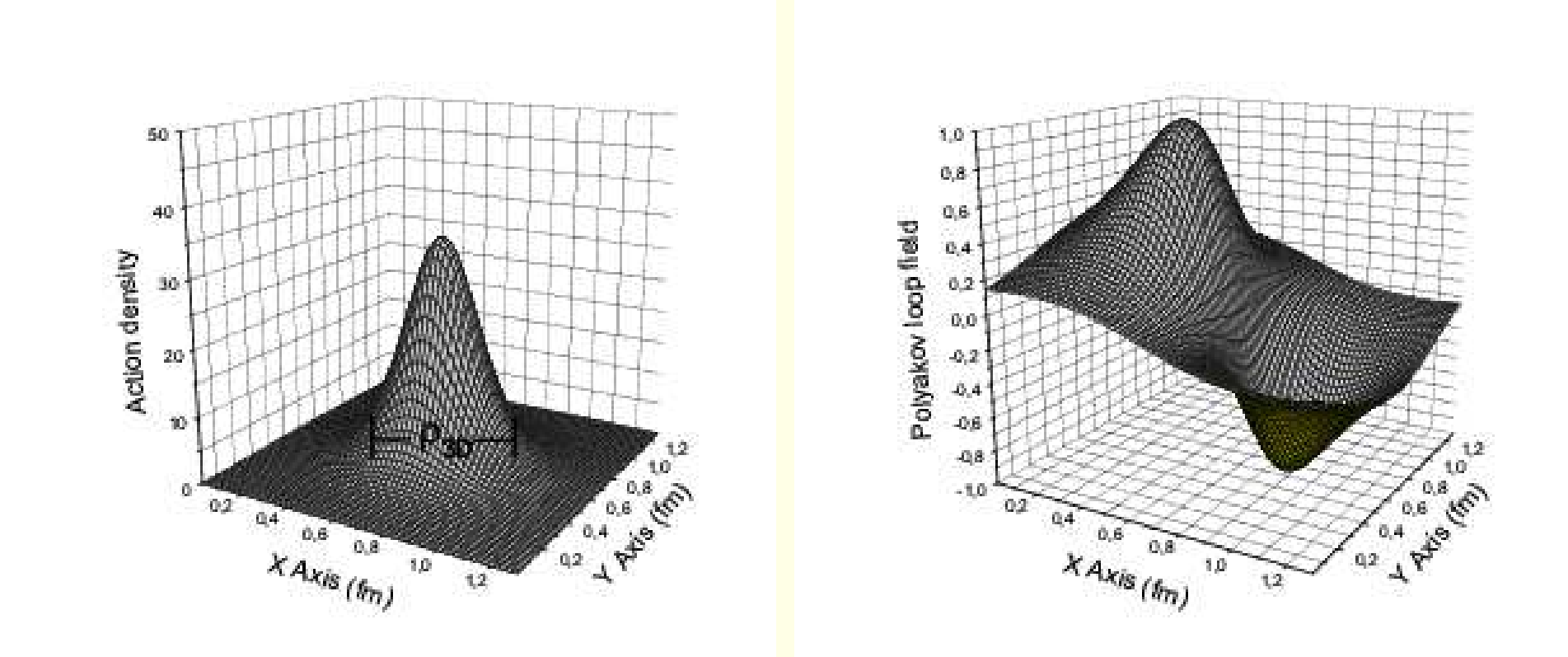

Figure 8: Action density (left) and Polyakov loop distribution (right) of a KvBLL caloron with maximally non-trivial holonomy $|\vec{\omega}| = 0.25$, $\rho = 0.33$ fm and $\beta = 1$ fm.

$SU(2)$: A large caloron: action density and Polyakov loop

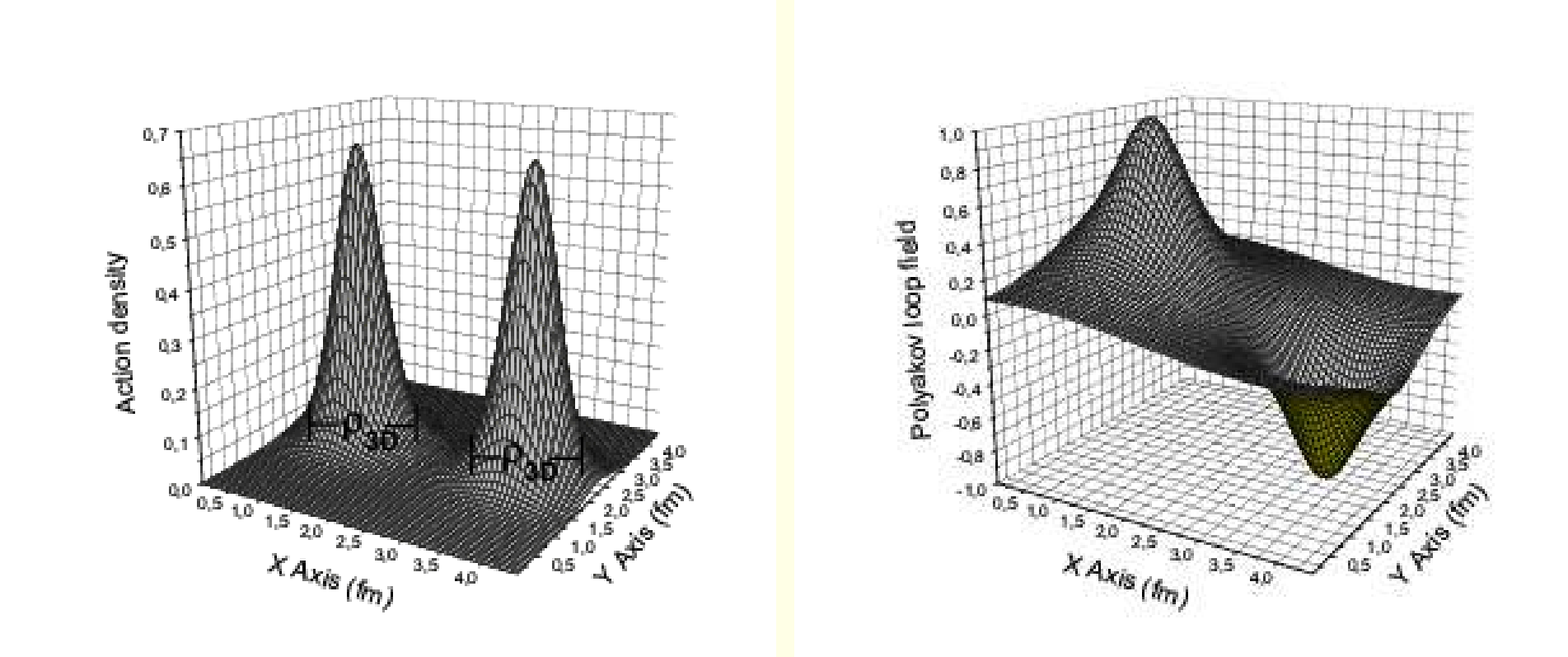

Figure 9: Action density (left) and Polyakov loop distribution (right) of a dissociated KvBLL caloron with maximally non-trivial holonomy $|\vec{\omega}| = 0.25$, $\rho = 1$ fm and $\beta = 1$ fm.

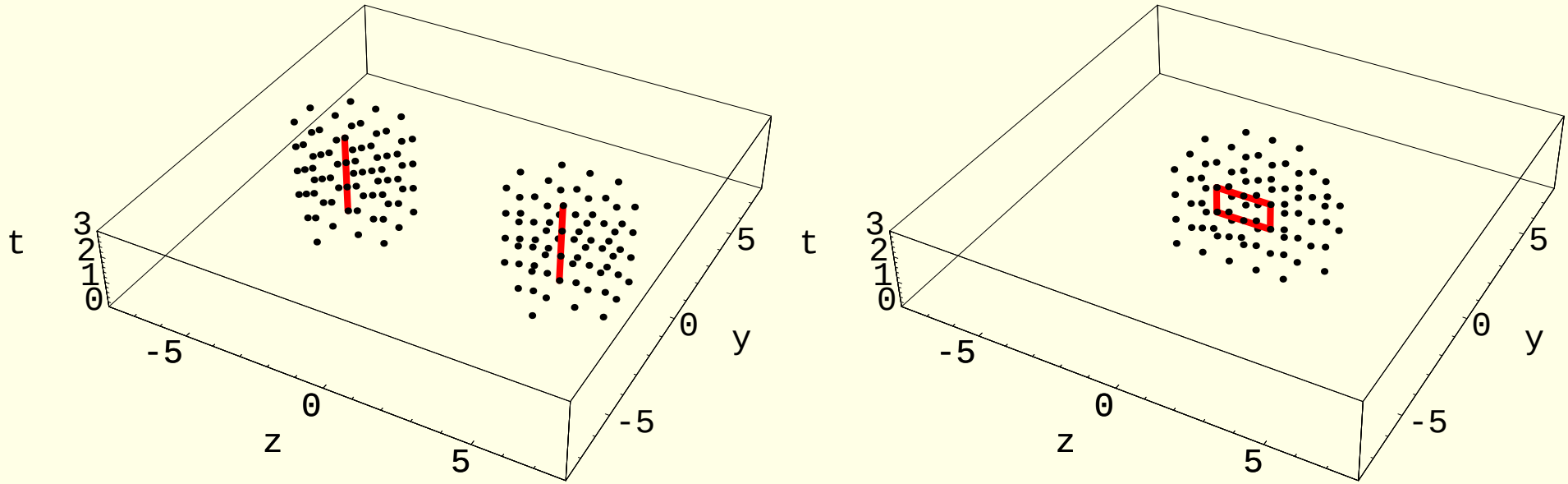

Figure 10: Left: two static dyons accompanied by two static Abelian monopoles; right: a single caloron accompanied by a monopole loop. The classical $SU(2)$ configurations have been generated on a $16^3 \times 4$ lattice and then Abelian-projected. In the (z, y, t) lattice at $x = 0$ we show the sites with action density $s > s_{\mathrm{max}}/5$ (left, for dyons) and $s > s_{\mathrm{max}}/40$ (right, for calorons) together with the emerging monopole trajectories.

Generic samples of $SU(3)$ calorons (as classical solutions) are obtained from confinement (not deconfinement !) ensembles by cooling (down to the action plateau) :

"Calorons in $SU(3)$ lattice gauge theory",
E.-M. I., M. Müller-Preussker, D. Peschka, Phys. Rev. D71, 116003 (2005)

This gives access to multi-calorons (of uniform selfduality or anti-selfduality, respectively), where the strict relation between topological charge and monopole number can be observed.

Wilson flow (being investigated now) detects non-classical structure !

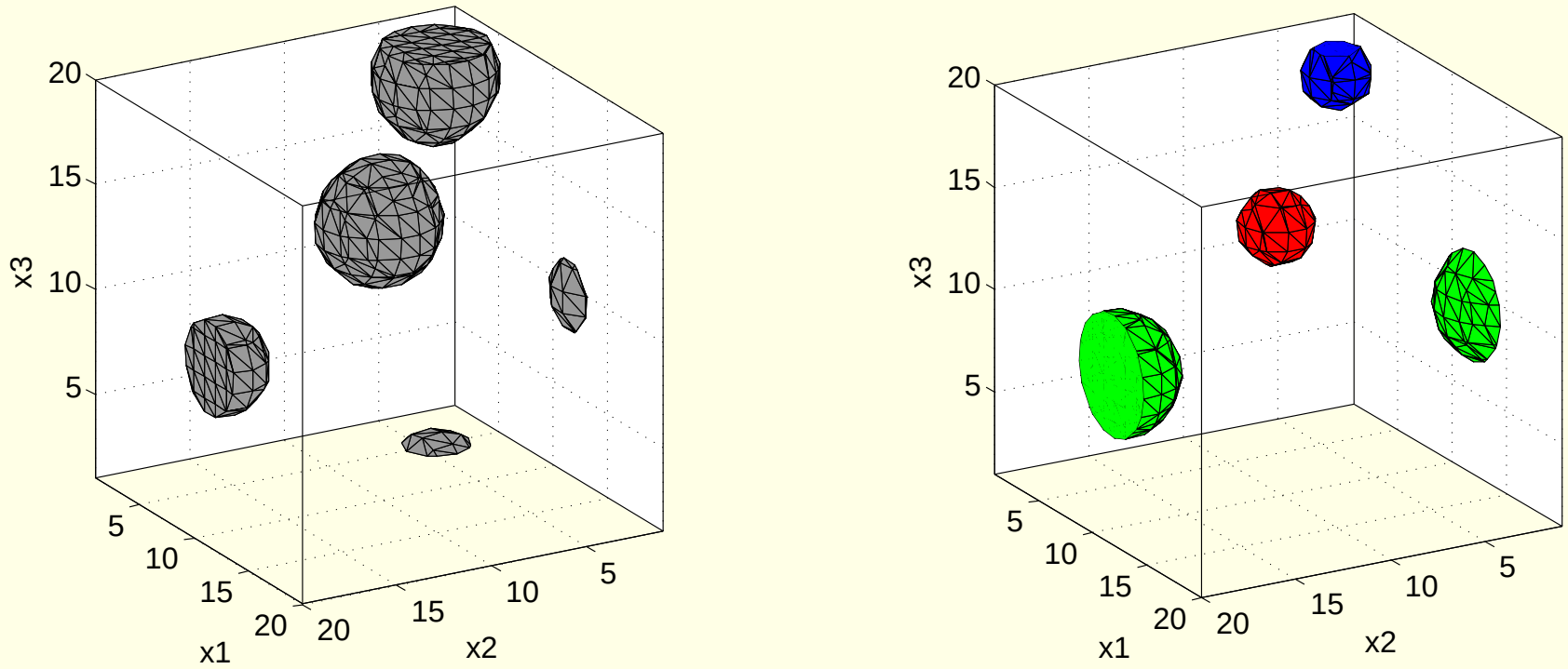

Figure 11: Caloron with non-trivial holonomy, topological charge $Q_t = -1$ and separated constituents. Isosurface plots are shown for the action density (left) and for the function $f(\vec{x})$ localizing the monopoles (right).

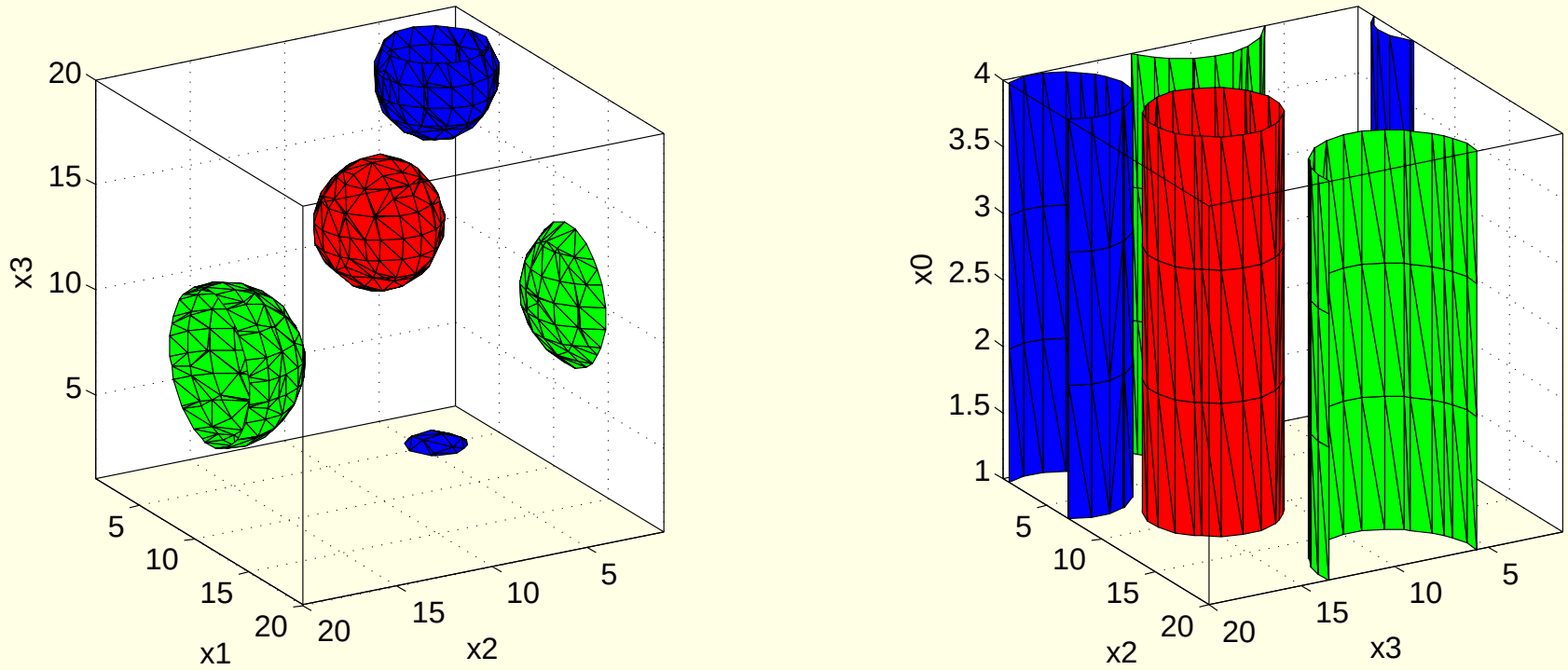

Figure 12: Isosurface plots are shown for the fermionic density $\Psi_z^\dagger \Psi_z(x)$ with boundary conditions $z = 1/6, 1/2, 5/6$ drawn with different colors at fixed x_0 (left) and fixed x_1 (right).

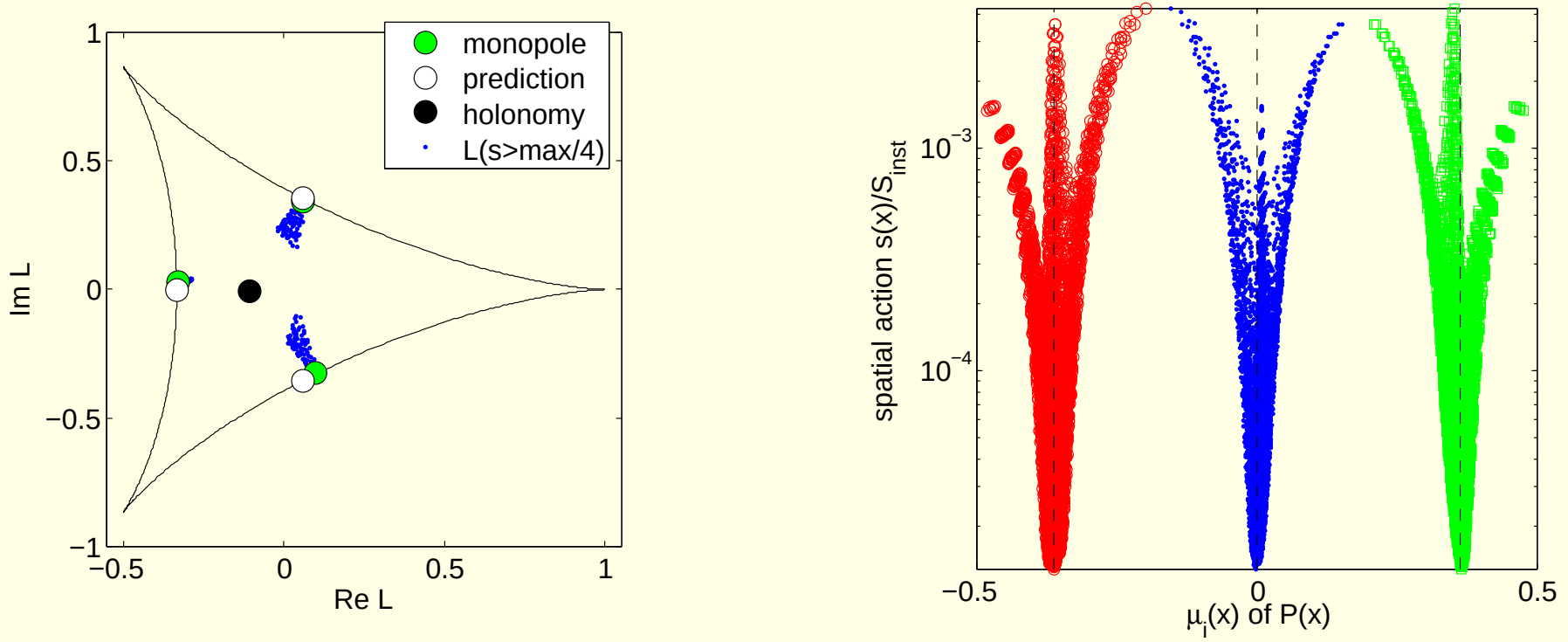

Figure 13: Non-trivial $Q_t = 1$ caloron. Left : scatterplot of $L(\vec{x})$ for points of high action density. Right : local eigenvalues of $\mathcal{P}(\vec{x})$ plotted vs. angle and spatial action density.

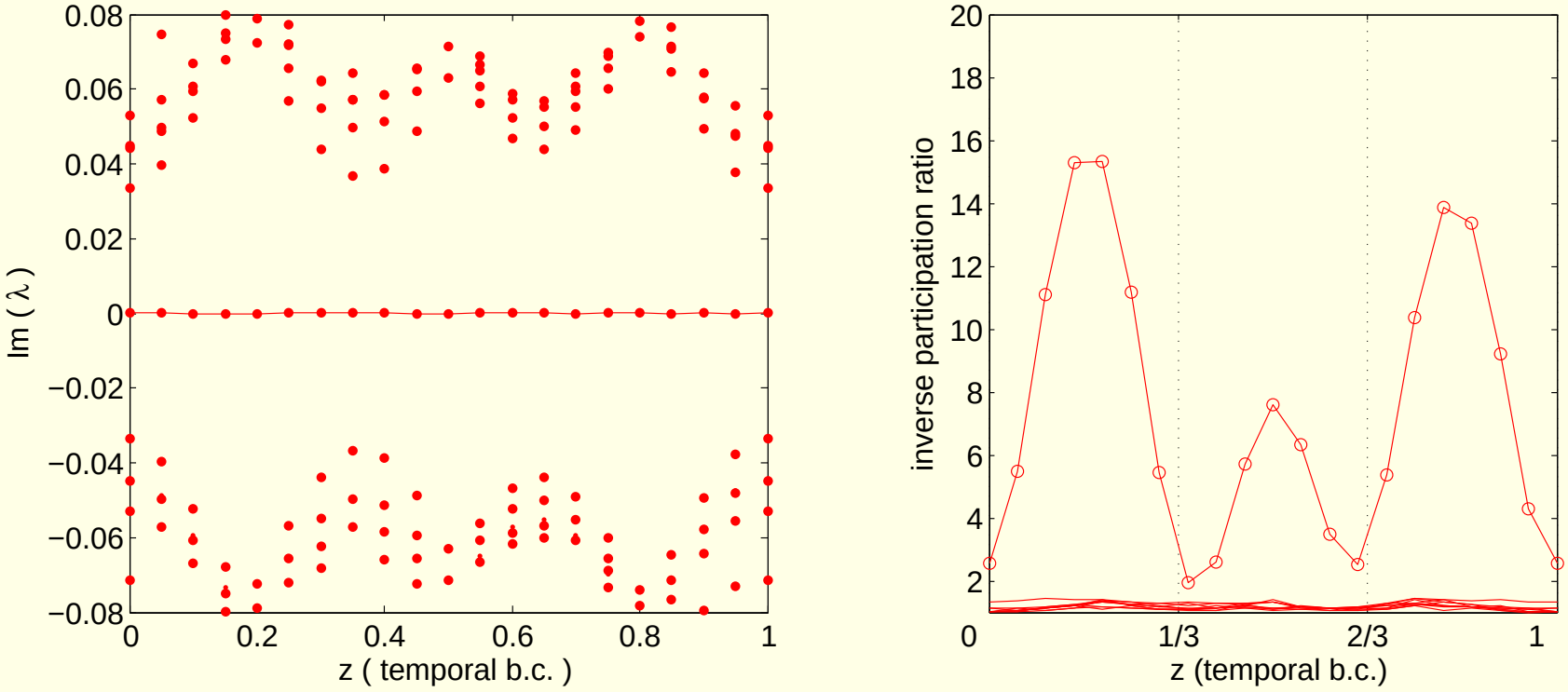

Figure 14: Non-trivial $Q_t = 1$ caloron : $\Im(\lambda)$ (four eigenvalues of D_{Wilson}) (left) and the IPR of the single zero mode (right) vs. angle z put into the boundary condition.

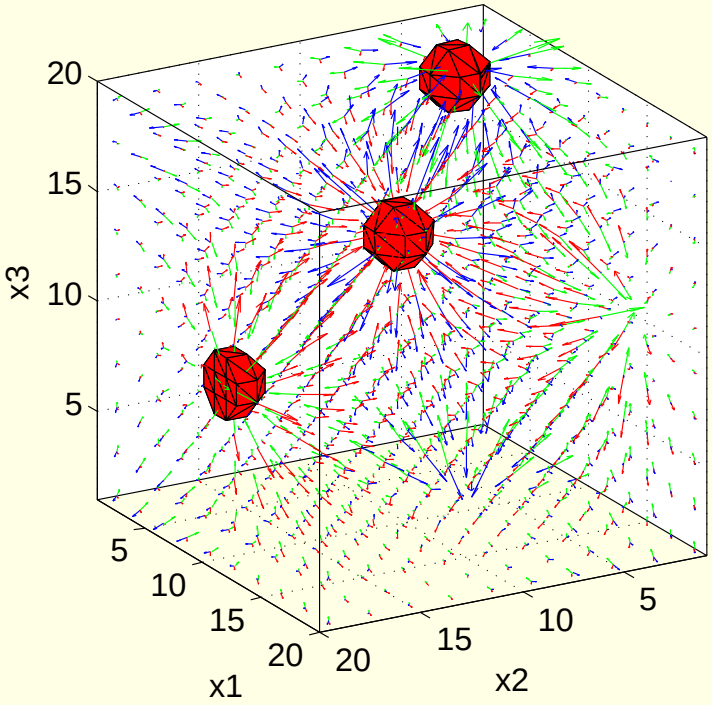

Figure 15: Abelian monopoles within a $Q = -1$ caloron with non-trivial holonomy and separated constituents; colored arrows show electric ($= -$magnetic) field components of Abelian projected $U(1) \times U(1)$ field. The isosurfaces show the action density of the Abelian projected field (i.e. the monopoles' non-Abelian interior).

III. Dyons in SU(3) below the transition and slightly above

1. Setup to generate configurations

   - lattice of size $20^3 \times 6$
   - pure $SU(3)$ gauge theory
   - Lüscher-Weisz action
   - robust overlap spectrum requires smooth configurations: changing the boundary condition should leave the index (number of zero modes) unchanged
   - Two ensembles (each 50 configurations) for the overlap analysis generated at $\beta = 8.20$ and $\beta = 8.25$
   - At essentially lower β (deeper in confinement) the reproducibility of the index would be lost.

Lüscher-Weisz action

$$S[U] = \beta \left(\sum_{pl} \frac{1}{3} \mathrm{Re\ Tr}[1 - U_{pl}] + c_1 \sum_{rt} \frac{1}{3} \mathrm{Re\ Tr}[1 - U_{rt}] + c_2 \sum_{pg} \frac{1}{3} \mathrm{Re\ Tr}[1 - U_{pg}] \right) ,$$

β is the principal inverse coupling parameter.

c_1 and c_2 are from one-loop perturbation theory and tadpole improvement:

$$c_1 = -\frac{1}{20 u_0^2}[1 + 0.4805\alpha] , \quad c_2 = -\frac{1}{u_0^2} 0.03325\alpha .$$

For any β, the tadpole factor u_0 and the lattice coupling constant α are self-consistently determined in terms of the average plaquette

$$u_0 = \left(\langle \frac{1}{3} \text{Re Tr } U_{pl} \rangle \right)^{1/4}, \quad \alpha = - \frac{\ln \left(\langle \frac{1}{3} \text{Re Tr } U_{pl} \rangle \right)}{3.06839}$$

in an iterative search.

Consider the distribution of the real part of the averaged Polyakov loop and of its modulus for the two ensembles:

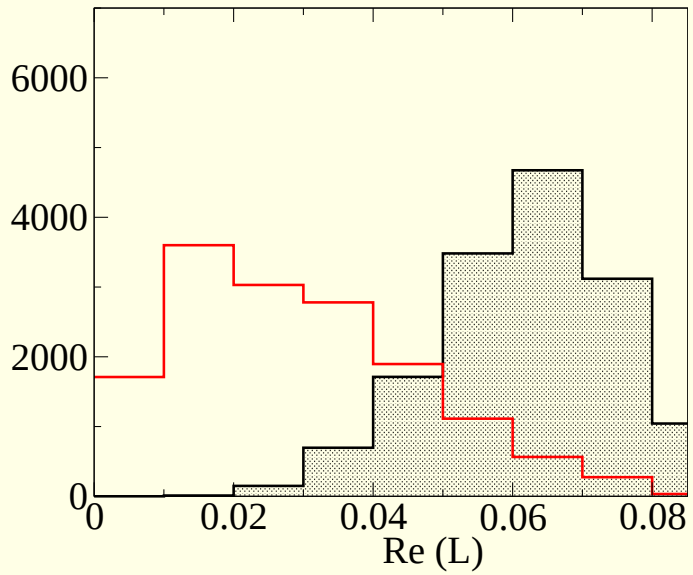

a)

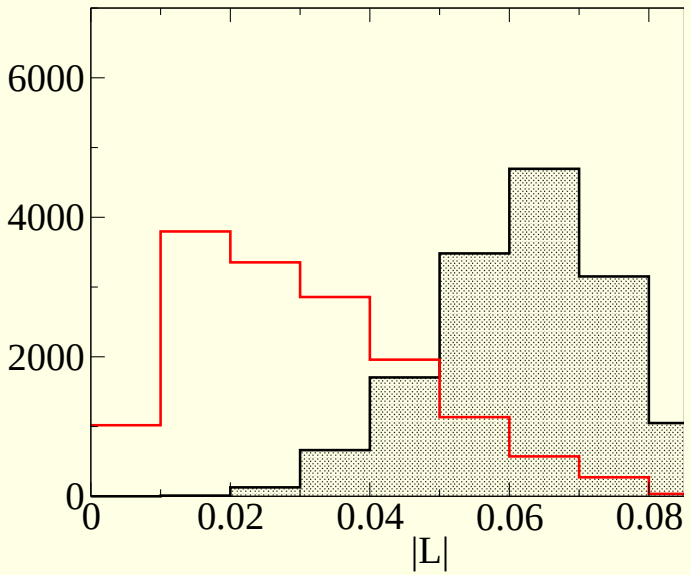

b)

Figure 16: The distributions a) of the real part of the spatially averaged Polyakov loop $Re(L)$ (eventually rotated to the real Z_3 sector) and b) of the modulus $|L|$, both at $\beta = 8.20$ (red curve) and $\beta = 8.25$ (shadowed), each based on a statistics of 15000 configurations.

This confirms :

- $\beta = 8.20$ belongs mainly to the confining phase (admixtures of deconfinement to be eliminated by Polyakov cuts, eventually).
- $\beta = 8.25$ exclusively belongs to the deconfining phase.

One might anticipate :

- Polyakov loop distributions at $\beta = 8.20$ and $\beta = 8.25$ are sufficiently different (taking this as "asymptotic holonomy") to produce noticeable differences in terms of dyons.
- However, the Polyakov loop modulus $|\overline{L}|$ is too small on the "deconfined side" to observe the full effect of the Polyakov loop on the dyon composition..

2. Overlap Dirac operator

The Neuberger operator is a solution of the Ginsparg-Wilson relation

$$D\gamma_5 + \gamma_5 D = \frac{a}{\rho} D\gamma_5 D \,,$$

As the input kernel we take the Wilson-Dirac operator,

$$D_{\mathrm{ov}} = \frac{\rho}{a}\left(1 + D_{\mathrm{W}}/\sqrt{D_{\mathrm{W}}^{\dagger}\ D_{\mathrm{W}}}\right) \,, \qquad D_{\mathrm{W}} = M - \frac{\rho}{a} \,.$$

D_{W} is the Wilson-Dirac operator with a negative mass term ρ/a, M is the Wilson hopping term with $r = 1$.

An optimal choice is $\rho \approx 1.4$.

For the sign function in the alternative expression

$$D_{\mathrm{W}}/\sqrt{D_{\mathrm{W}}^{\dagger}\ D_{\mathrm{W}}} = \gamma_5\ \mathrm{sgn}\,(H_{\mathrm{W}}) \,, \qquad H_{\mathrm{W}} = \gamma_5\ D_{\mathrm{W}} \,,$$

the minmax polynomial approximation (Giusti 2002) was used.

3. Topological charge density

The Pontryagin density can be expressed in the form

$$q(x) = -\mathrm{tr}\left[\gamma_5\left(1 - \frac{a}{2\rho}D_{\mathrm{ov}}(x,x)\right)\right] .$$

tr is the trace only over color and spinor indices.

This topological charge density contains vacuum fluctuations of all scales.

An ultraviolet filtered (mode-truncated) density is

$$q_{\lambda_{\mathrm{cut}}}(x) = -\sum_{|\lambda|\leq\lambda_{\mathrm{cut}}}\left(1 - \frac{\lambda}{2}\right)\psi^{\dagger}_{\lambda}(x)\gamma_5\psi_{\lambda}(x)$$

and shows conventional clustering of topological charge (instanton-like, dyons?). It resembles smearing:

Vacuum structure revealed by over-improved stout-link smearing compared with the overlap analysis for quenched QCD, Phys. Rev. D77:074502 (2008) [arXiv:0801.1725], E.-M. I., D. Leinweber, P. Moran, K. Koller, G. Schierholz, V. Weinberg.

4. Modified boundary conditions and Dirac spectrum

For the improved action in the β range under investigation, the index is unchanged and the spectrum approximately unchanged under a change of boundary conditions.

In $SU(2)$ we used antiperiodic and periodic boundary conditions to map out clusters of topological charge with the required sign of the local Polyakov loop (holonomy).

Here, we select three angles for use in the boundary conditions: two complex ones, and the antiperiodic one.

$$\psi(1/T) = \exp(i\phi)\psi(0)$$

with

$$\phi = \begin{cases} \phi_1 \equiv -\pi/3\,, \\ \phi_2 \equiv +\pi/3\,, \\ \phi_3 \equiv \quad \pi\,. \end{cases}$$

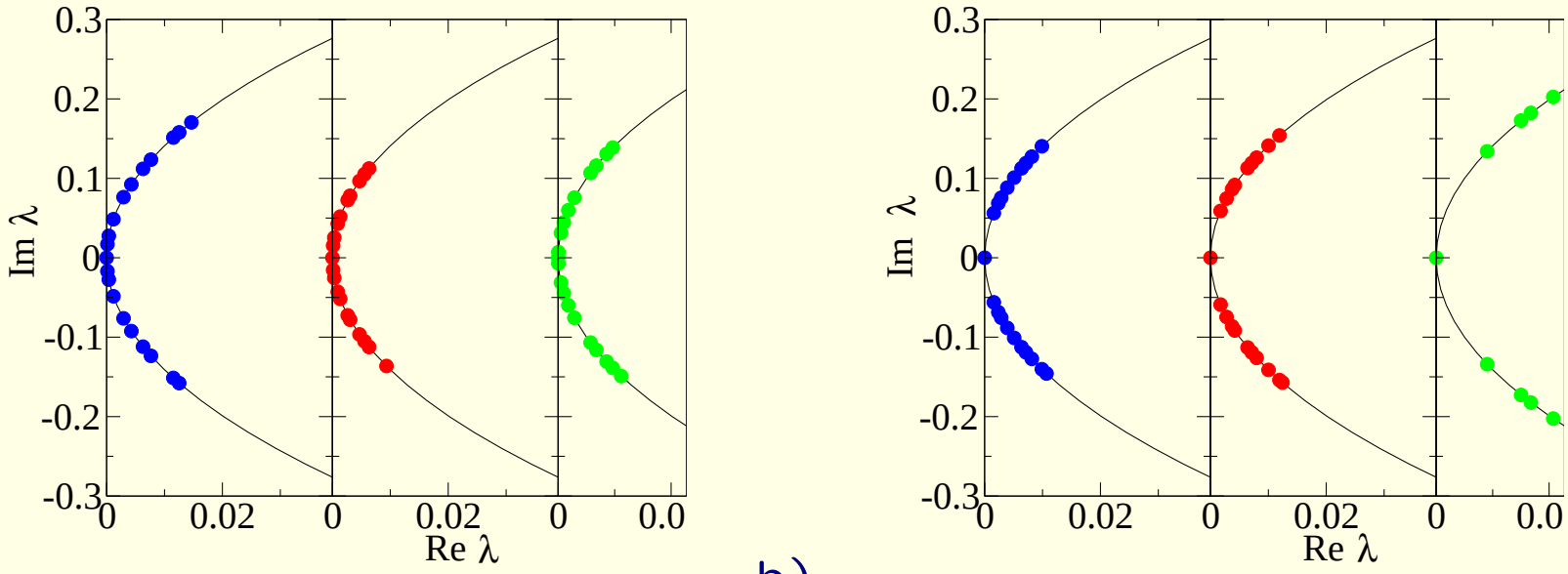

a) b)

Figure 17: For two typical configurations and in each case for the three versions of the fermion temporal b.c. the 20 lowest eigenvalues of the $SU(3)$ overlap Dirac operator are shown, for a) $\beta = 8.20$ and b) $\beta = 8.25$, respectively. In both of the panels for $\phi = \phi_1$ the spectrum is shown left (in blue), for $\phi = \phi_2$ in the middle (in red), and for $\phi = \phi_3$ (antiperiodic b.c.) it is plotted right (in green), respectively.

5. Three (selective) topological densities instead of one (gluonic)

We have reconstructed from the zero and the non-zero modes the profiles of the UV-filtered topological charge density, detailed for the three boundary conditions, according to its spectral representation

$$q_{i,N}(x) = -\sum_{j=1}^{N} \left(1 - \frac{\lambda_{i,j}}{2}\right) \psi^{\dagger}_{i,j}(x)\gamma_5\psi_{i,j}(x)\,,$$

where j enumerates the eigenvalues $\lambda_{i,j}$ equal and closest to zero. These eigenvalues $\lambda_{i,j}$, as well as the corresponding modes $\psi_{i,j}(x)$, are also characterized by the i-th boundary condition. Correspondingly, the UV-filtered topological density $q_{i,N}(x)$ depends on the boundary condition, too.

6. Cluster analysis of the three charge densities

Cluster analysis with a variable lower cut-off $q_{\mathrm{cut}} > 0$:

- first step: the algorithm identifies the interior of all clusters ("topological cluster matter") as the region where $|q(x)| > q_{\mathrm{cut}}$.
- crucial next step: enquire connectedness between the lattice points in order to form individual clusters out of this "cluster matter".
  Neighbouring points with $|q(x)|$ above threshold and sharing the sign of topological density belong to the same cluster.
- choice of the cut-off q_{cut}: made such as to decompose the "continuous" distribution into a maximal number of internally connected clusters, being mutually separated (q_{cut} is independently adapted for each configuration).

The purpose of the cluster analysis was to discover extended objects as dyon candidates of different kind in order to study their "space-time coordination" and Polyakov line profiles.

Later, well above the deconfinement transition, also their relation to the Maximal Abelian gauge monopoles has been investigated.

7. Abundances of the three sorts of clusters

Lower temperature

- For the lower temperature ($\beta = 8.20$) we have found the following average numbers of clusters per configuration :

$$N_1 = 18.4(0.4), \quad N_2 = 18.6(0.5), \quad N_3 = 16.6(0.3)\,.$$

- The nomenclature corresponds to the configuration being rotated (by a $Z(3)$ flip) into the real $Z(3)$ sector (such that the average Polyakov loop has $-\pi/3 < \arg(\overline{L}) < \pi/3$) if needed.
- N_1 and N_2 are coinciding within errors, while N_3 is slightly lower.
- The average size of all clusters amounts to 146 lattice points.
- However, the abundance of all three types of clusters should be equal for confining configurations.

- Assuming the lattice scale fixed by the transition temperature for $SU(3)$ gluodynamics ($T_c \approx 300$ MeV) we estimate the physical dyon cluster density:

$$\rho \approx 6 \text{ fm}^{-4}$$

.

- The observed slight asymmetry $N_3 < N_1 = N_2$ might be due to the admixture of configurations related to deconfinement.
- We applied a Polyakov cut for the modulus $|\overline{L}| < 0.3$ and get the corrected multiplicities:

$$N_1 = 17.8(0.6), \quad N_2 = 18.3(0.6), \quad N_3 = 17.2(0.5)\,.$$

- The inverse participation ratios (IPR) calculated for the zero modes for three types of b.c.'s turn out to be

$$IPR_1 = 6.8(0.8),\ IPR_2 = 6.4(1.0),\ IPR_3 = 15.2(1.7),$$

- Having applied the above mentioned cut for $|\overline{L}|$ we find

$$IPR_1 = 5.8(0.9),\ IPR_2 = 5.0(0.6),\ IPR_3 = 8.5(0.6)\,.$$

Critique :

Even with this cut taken into account, an asymmetry of multiplicities and IPR seems still to exist, but is far less pronounced.

Temperature slightly higher: onset of statistical suppression of "heavy dyons" ?

- Average number of clusters

$$N_1 = 20.7(0.6), \quad N_2 = 20.6(0.6), \quad N_3 = 17.1(0.4)$$

  reflecting the different distribution of $\overline{L}$.

- The asymptotic holonomy would (for an exact caloron) provide the dyon constituents corresponding to antiperiodic fermionic boundary conditions with a higher action.

- Average size of these clusters amounts to 172 lattice points (20 percent larger in lattice units).

- Density of clusters is higher than at lower temperature:

$$\rho \approx 8 \text{ fm}^{-4}$$

  .

- A more pronounced asymmetry is seen in the IPR of zero modes:

$$IPR_1 = 7.9(0.8),\ IPR_2 = 7.2(0.7),\ IPR_3 = 24.6(1.8).$$

For antiperiodic b.c. all low modes are localized about three times more than modes sitting on "light dyons".

Conclusion :

Changes go in the expected direction :

- "heavy dyons" are more suppressed
- the number density of "dyons" is increased
- light clusters become larger in space-time
- heavy clusters are much (!) more concentrated
- alternatively characterize the actually heavy dyons according to
  having "their" Polyakov loop opposite to the trivial one ?

8. Inter-cluster correlations

Lower temperature

$$\begin{aligned} \text{number of isolated clusters} &= 1299 \quad (49\%), \\ \text{number of clusters in pairs} &= 782 \quad (29\%), \\ \text{number of clusters in triplets} &= 597 \quad (22\%), \end{aligned}$$

We see full caloron-like clusters and completely dissolved caloron constituents coexisting in this ensemble.

Temperature slightly higher

$$\begin{aligned} \text{number of isolated clusters} &= 1600 \quad (55\%), \\ \text{number of clusters in pairs} &= 834 \quad (28\%), \\ \text{number of clusters in triplets} &= 492 \quad (17\%). \end{aligned}$$

Conclusion : at this temperature the amount of fully dissociated dyons has grown at the expense of dyons enclosed in clusters of three dyons (calorons ?).

9. Clouds of topological charge plotted vs. Polyakov loop

Result :

- Calorons interconnect the three sides
- Dyon pairs interconnect two sides
- Isolated dyons are located close to one side (monopoles)

of the Polyakov triangle.

The sides correspond to the three angles ϕ_i.

This result is as expected.

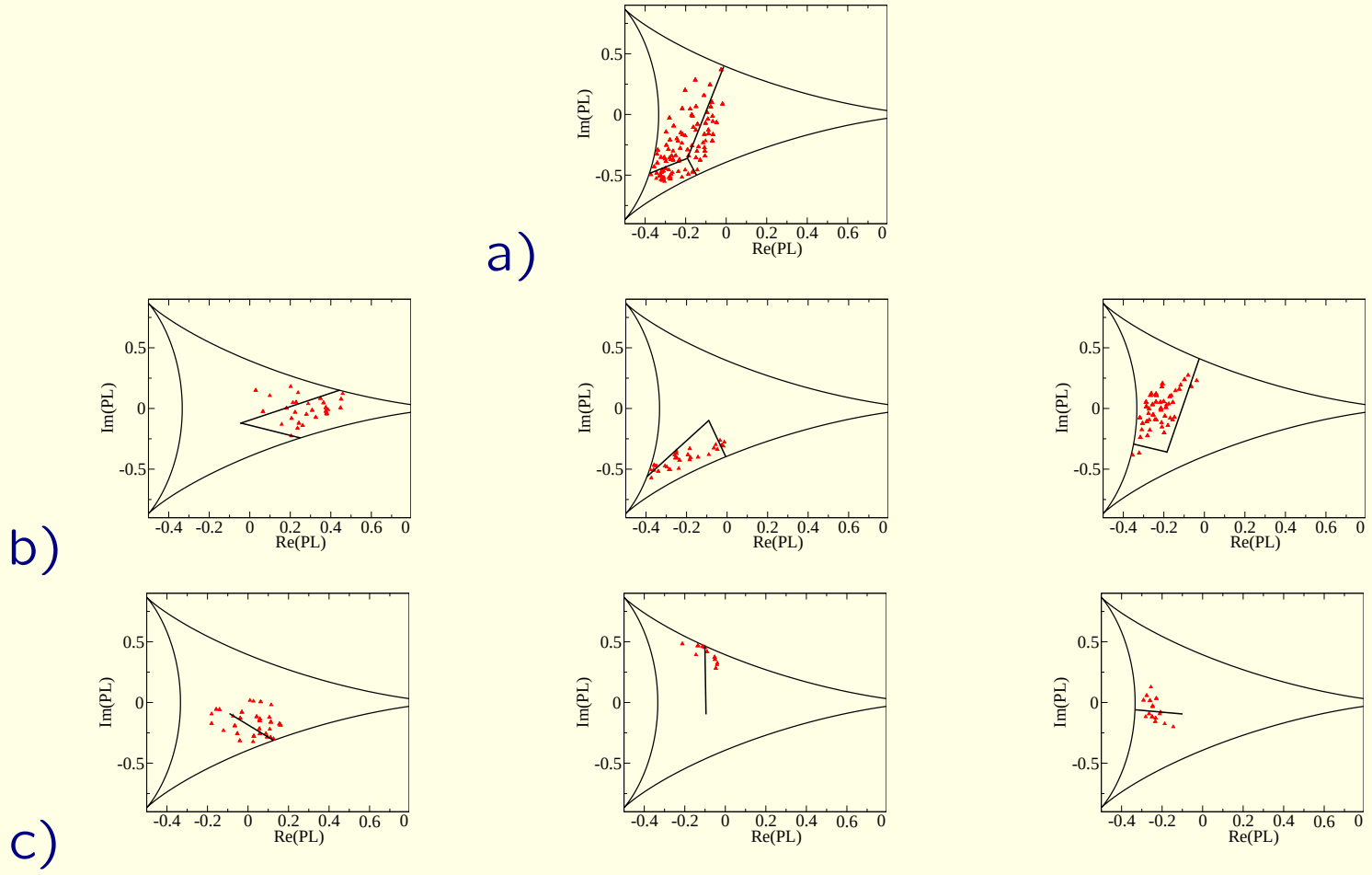

Figure 18: The profile of the local Polyakov loop L in examples of topological "clouds" formed a) by a triplet of clusters (top), b) by (three types of) cluster pairs (middle) and c) consisting of (three types of) isolated clusters (bottom). This pattern obtained for $\beta = 8.20$ is characteristic for the confining phase. In the figures straight lines are connecting the point representing the averaged Polyakov loop $\overline{L}$ of the cooled configuration and the point or points representing the local Polyakov loop $L(\vec{x})$ in the respective dyon center(s).

10. Polyakov line portraits of configurations in terms of clusters : is this an additional indication in favor of the dyon nature ?

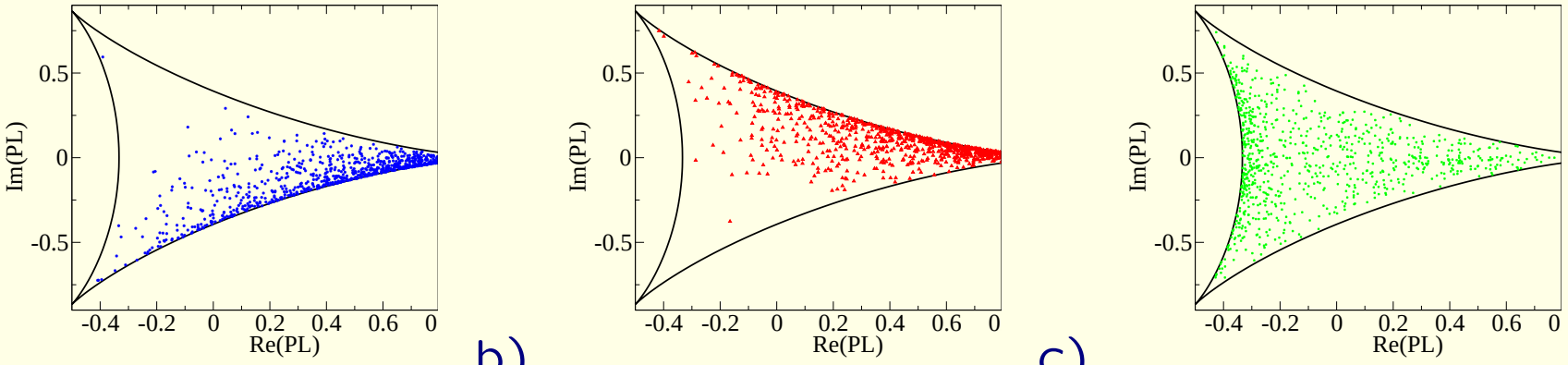

Figure 19: For three cases of the fermion temporal b.c., the zero and near-zero modes of $SU(3)$ overlap Dirac operator define three different profiles of the topological charge density on a configuration belonging to the ensemble at $\beta = 8.20$ ($T \simeq T_c$). Each cluster of these profiles is represented in the plots by the Polyakov loop $L(\vec{x})$ measured in its cluster center. The ordering corresponds to spatially averaged Polyakov loop rotated into the real $Z(3)$ sector (after improved cooling). a) 918 clusters of first type (blue), b) 929 clusters of second type (red), c) 831 clusters of third type (green).

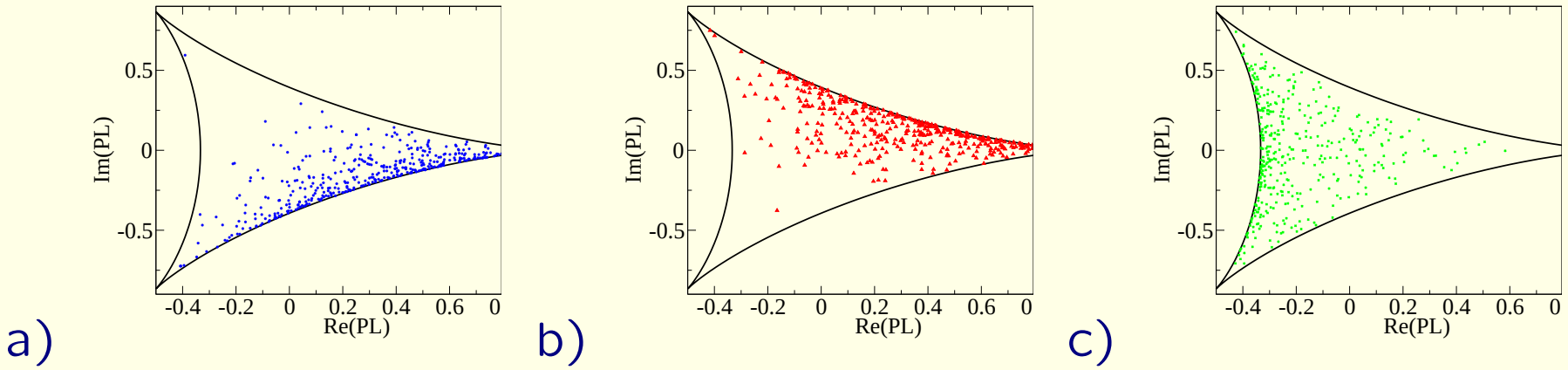

Figure 20: Same as in Fig. 19 but with a cut $|\overline{L}| < 0.3$ (after improved cooling, emphasizing the confining part of the ensemble) leaving only 23 (out of 50) configurations. a) 409 clusters of first type (blue), b) 421 clusters of second type (red), c) 395 clusters of third type (green).

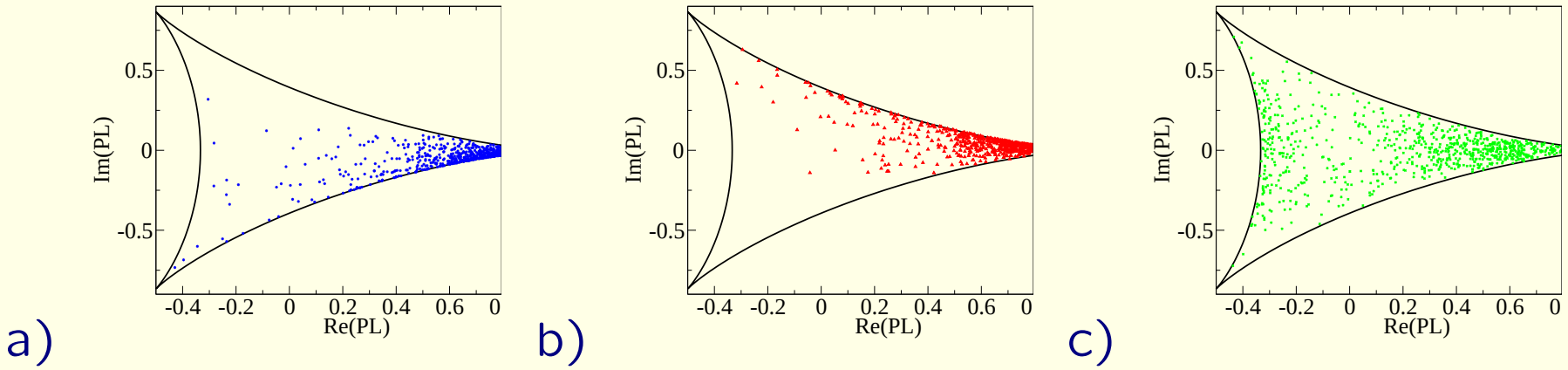

Figure 21: The analogous plot for the ensemble at $\beta = 8.25$ ($T \gtrsim T_c$). a) 1036 clusters of first light type (blue), b) 1032 clusters of second light type (red), c) 858 clusters of heavy type (green).

Except for part of the type-3 clusters, just above T_c clusters of all types increasingly gather in the trivial center (rightmost) corner.

11. Overimproved cooling – a useful method for identifying the phase and the topological density !

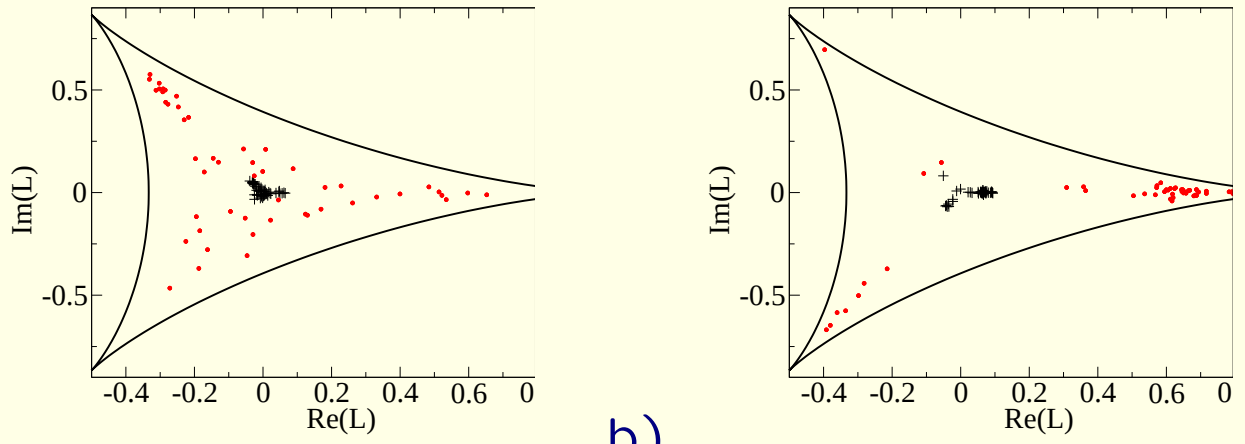

Figure 22: Ensemble scatter plots of the spatially averaged Polyakov loop $\overline{L}$ before (black crosses) and after cooling (red dots) for a) $\beta = 8.20$ and b) $\beta = 8.25$, respectively.

Below T_c, under cooling the average Polyakov loop "explodes" isotropically, above T_c preferentially into the trivial directions.

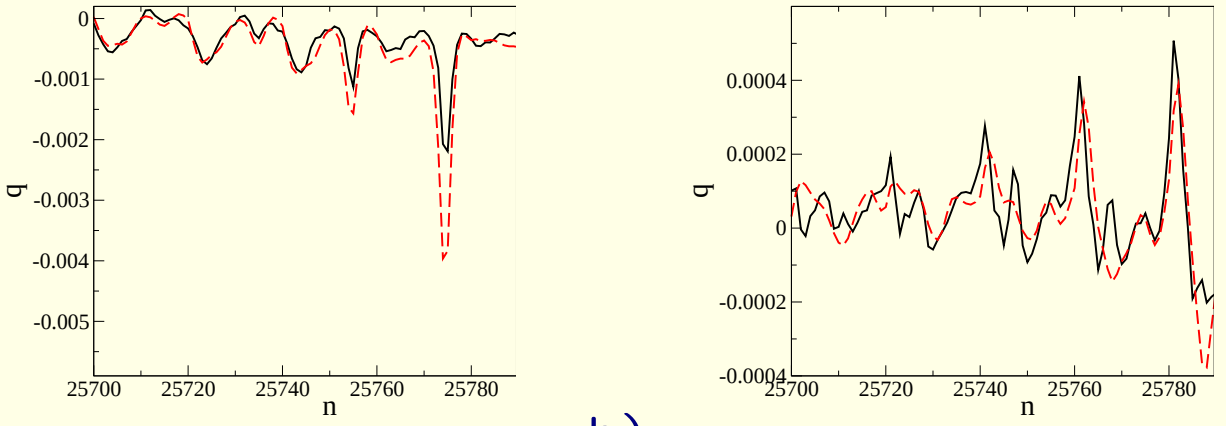

a) b)

Figure 23: Comparison (along some string of lattice sites) of the overlap topological charge density of a typical configuration for a) $\beta = 8.20$ and b) $\beta = 8.25$ (averaged over b.c.'s, shown as solid black line) with the gluonic topological charge density (dashed red line). The latter is determined after an optimized number of overimproved cooling steps.

A somewhat better agreement can be achieved for confinement ($\beta = 8.20$) than for deconfinement ($\beta = 8.25$).

Remarks

The idea to confront the filtering provided by a given cut-off in analyzing modes with the filtering effected by overimproved stout link cooling (at $T = 0$) was the guiding idea of the paper

E.-M. I., D. Leinweber, P. Moran et al., Phys.Rev. D77 (2008) 074502, arXiv:0801.1725

Extended to $O(50)$ cooling steps and matching to the corresponding cut applied to the overlap modes, both techniques agreed to detect bigger topological lumps (with instanton properties) at the corresponding scale.

Searching for instanton constituents ("instanton quarks") was not within the scope of that paper. This (as we know now) requires a smaller smearing scale.

The present comparison has lead us to conclude that after ≈ 20 cooling steps the gluonic topological density approaches best the UV-filtered overlap topological density (based on 20 modes).

Next steps :

More systematical analysis applying Wilson's gradient flow !

VI. The dyonic picture deeper in deconfinement

Setup to generate configurations

- Lattice of size $20^3 \times 4$ instead of $20^3 \times 6$
- Pure $SU(3)$ gauge theory with Lüscher-Weisz action
- ... with a robust overlap Dirac spectrum
- An ensemble (with 50 configurations) is generated at $\beta = 8.25$: corresponding to $T \approx 1.5\ T_{\mathrm{dec}}$
- 20 lowest non-zero modes have been included in the analysis
- For comparison, we have also used less (10) non-zero modes
- Gauge fixing to the Maximally Abelian gauge (Simulated annealing with 10 gauge copies per configuration to choose the maximal gauge functional)

- Localizing thermal monopoles (following Brandstaedter, Schierholz, Wiese et al., Bornyakov et al. DIK Collaboration)
- For studying the Polyakov line profile we have used 4 steps of overimproved cooling
- After 4 cooling steps, the gluonic topological charge coincides with the index of the overlap Dirac operator within 10 %.

a)

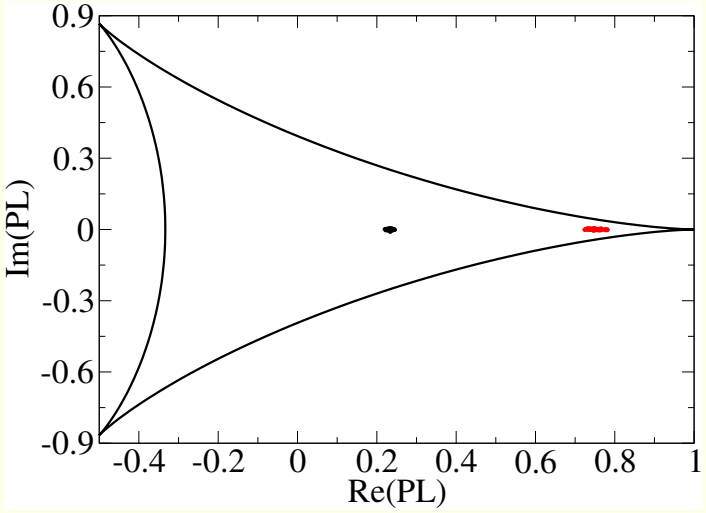

b)

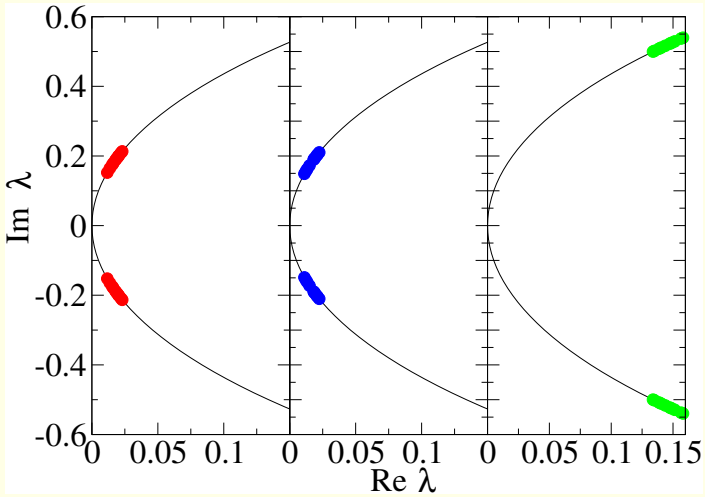

Figure 24: a) Scatter plots of the spatially averaged Polyakov loop $\overline{L}$ for 50 Monte-Carlo generated configurations (black symbols at $\overline{L} \simeq 0.24$; the right group of red points shows the evolution of $\overline{L} \rightarrow\simeq 0.75$ after four steps of over-improved cooling), b) overlap eigenvalues for one of these configurations under the three boundary conditions.

Global topology at $T = 1.5\ T_{\mathrm{dec}}$:

The ensemble of 50 configurations has only 7 configurations with $Q_{index} \neq 0$.

The topological susceptibility is estimated as $\chi_t = \langle Q^2_{index} \rangle / V \simeq (82\ \mathrm{MeV})^4$.

Topological clusters and Abelian monopoles :

The three-dimensional projection of points belonging to topological clusters and the location of the (static) monopole loops after four sweeps of over-improved cooling steps are visualized as follows:

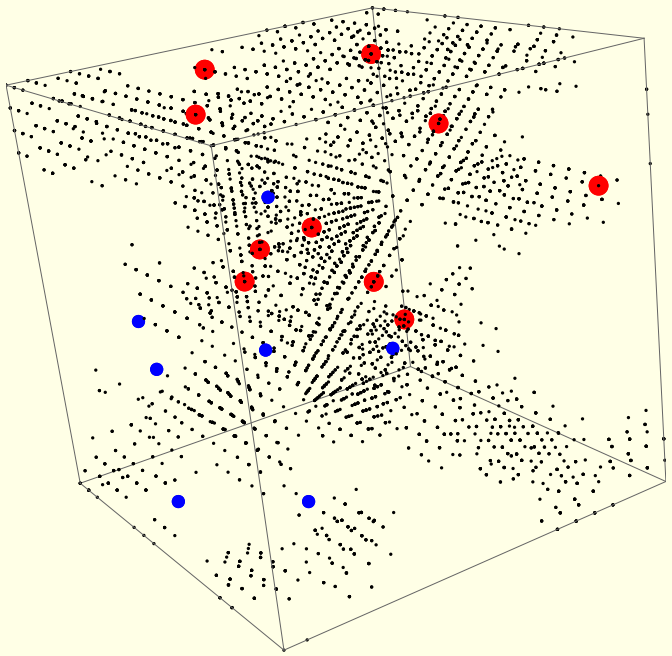

Figure 25: The three-dimensional projection of points belonging to topological clusters (black small points) and the location of static time-like monopole loops after moderate over-improved cooling inside clusters (larger red spheres) and outside clusters (small blue spheres) are shown for one typical Monte Carlo generated gauge field configuration.

Main results concerning the correlation between topological clusters and MAG monopoles

- Topological clusters are found to attract MAG monopoles .
- Classically, single dyons can be shown to appear as MAG monopoles.
- In the quantum ensemble, 16.8 % of volume are occuped by clusters (packing fraction), 9.7 % by clusters with monopoles.
- In the quantum ensemble, 35 % of monopole world lines are passing through topological clusters.
- In the quantum ensemble, 50 % of wrapping monopole world lines ("thermal monopoles") are passing through topological clusters.
- Clusters of third type are in one-to-one correspondence with Abelian monopoles.

- The suppression of heavy (third type) clusters compared to others can be expressed through the abundance ratios of MAG monopoles:

$$14 : 12 : 3.6$$

- The size of clusters with MAG monopoles is an order of magnitude larger than the size of others.
- The abundance of clusters with MAG monopoles is an order of magnitude less than the number of others.
- Clusters of third type (heavy dyons) are pierced just by one monopole world line. So, these dyons can be thought of as distinguished from other (light) dyons.
- Clusters of first and second types (light dyons) : approximately half of them are pierced by two monopole loops.

- Depending on their local Polyakov loop far from the real corner, clusters of third type can be "heavy" (carry more action and topological charge).
- Clusters of first and second type correlated with Abelian monopoles are "light" (carry small action and topological charge).
- Light topological clusters correlated with thermal monopoles are localized at the border of the Polyakov triangle closer than at lower temperature (i. e. two holonomy eigenvalues are nearly degenerate).

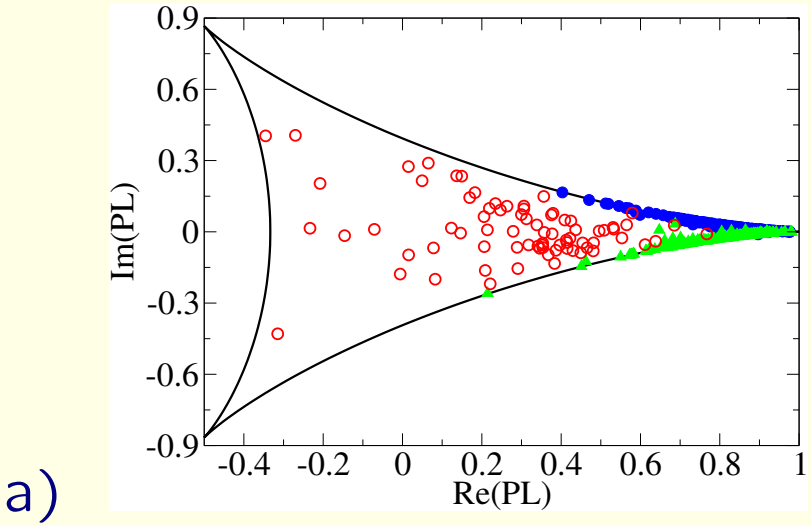

a)

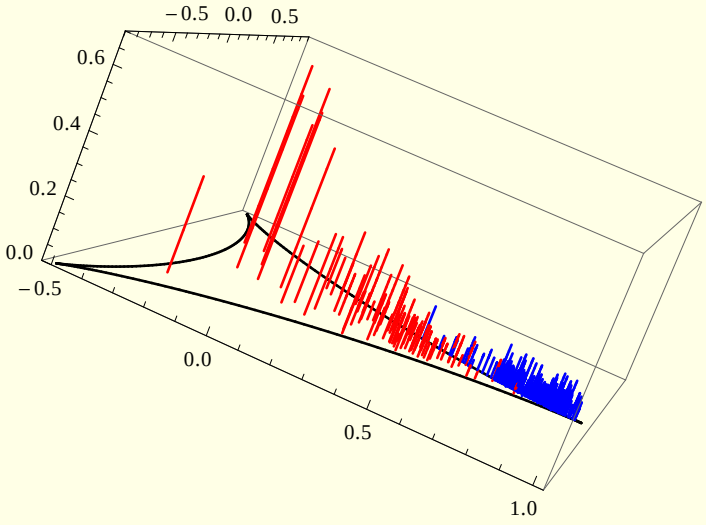

b)

Figure 26: a) Scatter plots of Polyakov loop L (after 4 steps of cooling) in clusters selected to contain monopoles, separated according to the type of boundary condition for the overlap near-zero modes. For clusters of first type the Polyakov loop is shown by green triangles, for clusters of second type - by blue filled circles, for clusters of third type - by red open circles; b) The maximum of the topological density inside the respective cluster is additionally shown as spikes in respective color (for second [blue] and third [red] type clusters only).

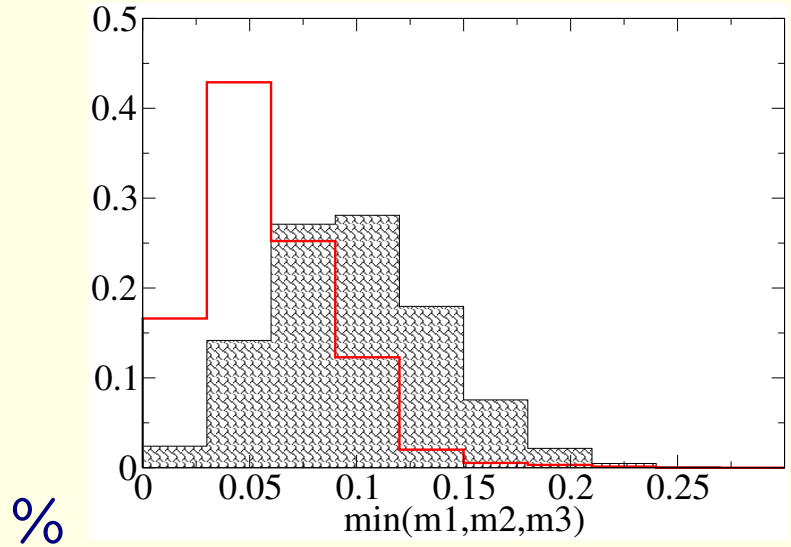

Figure 27: For all lattice points (shaded histogram) on one hand and for all cubes where thermal monopoles are located (open red histogram) on the other hand, the respective distribution with respect to the minimal distance $\min(m_1, m_2, m_3)$ between the Polyakov loop and one of the boundaries of the Polyakov triangle is shown. In the case of monopoles the minimum is taken also among the 8 corners of the three-dimensional cube contaning the monopole.

VII. Summary and outlook

- We have recalled a series of attempts to clarify (by means of simulation) the envisaged contribution of dyons to confinement.
- Recently, our method to detect (in Monte-Carlo generated lattice configuration) clusters of topological charge has made use of modified temporal boundary conditions to the overlap Dirac operator.
- Again, the topological structure turns out to be a scale-dependent concept !
- A finite number of analysing modes, respectively the number of (overimproved) cooling steps, introduces scale-dependence in our analysis.
- We shall repeat this analysis using Wilson's gradient flow and the corresponding definition of the infrared scale.

This study has provided a qualitative difference between the confinement phase (and close to the transition) and the topological structure at $T \approx 1.5 T_{\rm dec}$ formulated as a "light plus heavy dyonic picture" :

- Close to the transition, the changes in the supposed "dyon structure" are less obvious than expected : the "heavy dyon suppression" is still weak. A weakly first order transition !
- The dyonic picture at higher temperature shows strong differences between topological clusters selected according to different fermionic boundary conditions:
  1. abundance of heavy dyons is suppressed
  2. heavy dyons are $10\times$ more localized
  3. heavy dyons are in one-to-one correspondence to thermal MAG monopoles
  4. light dyons are less correlated to thermal MAG monopoles

Previous papers of our group related to dyon structure :

- Search for calorons and dyons in lattice configurations
  - Calorons and dyons at the thermal phase transition analyzed by overlap fermions,

    V.G. Bornyakov, E.-M. I., B.V. Martemyanov, S.M. Morozov, M. Müller-Preussker,

    A.I. Veselov, Phys. Rev. D76:054505 (2007) [arXiv:0706.4206 [hep-lat]]
  - The Topological structure of SU(2) gluodynamics at $T > 0$: An Analysis using the

    Symanzik action and Neuberger overlap fermions,

    V.G. Bornyakov, E.V. Luschevskaya, S.M. Morozov, M.I. Polikarpov, E.-M. I.,

    M. Müller-Preussker, preliminary results in PoS LAT2007:315 (2007)

    Phys. Rev. D79:054505 (2009) [arXiv:0807.1980 [hep-lat]]
  - The dyonic picture of topological objects in the deconfined phase,

    V.G. Bornyakov, E.-M. I., B.V. Martemyanov, M. Müller-Preussker,

    Phys. Rev. D79:034506 (2009) [arXiv:0809.2142 [hep-lat]]

- Model building
  - Confinement from a caloron gas

    An SU(2) KvBLL caloron gas model and confinement,

    P. Gerhold, E.-M. I., M. Müller-Preussker,

    Nucl. Phys. B760:1 (2007) [arXiv: hep-ph/0607315]
  - Sign problem from the moduli metric of the dyon model !

    Cautionary remarks on the moduli space metric for multi-dyon simulations,

    F. Bruckmann, S. Dinter, E.-M.I., M. Müller-Preussker, M. Wagner,

    Phys. Rev. D79:116007 (2009) [arXiv: 0903.3075 [hep-ph]]
  - Confinement from a random dyon gas !

    Confining dyon gas with finite-volume effects under control,

    F. Bruckmann, S. Dinter, E.-M.I. B. Maier, M. Müller-Preussker, M. Wagner,

    Phys. Rev. D85:034502 (2012) [arXiv: 1111.3158 [hep-ph]]

    Ewald summation is necessary to sum the Coulomb-like dyon fields !

The correlator of the Polyakov loop

$$P(\vec{r}) = -\sin\left(\frac{\Phi(\vec{r})}{2T}\right)$$

where Φ is built up from contributions of randomly placed dyons

$$\Phi(\vec{r}) = \sum_j \frac{q_j}{|\vec{r} - \vec{r}_j|}$$

has the form

$$\langle L(\vec{r}) L(\vec{r}') \rangle \propto \left(-\frac{\pi\ d\ \rho}{2\ T^2}\right)$$

this gives a linearly rising pair free energy

$$F_{Q\bar{Q}} = \sigma\ d + const$$

with a "string tension"

$$\sigma = \frac{\pi\ \rho}{2\ T}$$

proportional to $\rho =$ three-dimensional dyon density

- Vortex structure is found in $SU(2)$ calorons, and vortex confinement may happen in multicaloron gases

  Vortex structure of SU(2) calorons,

  F. Bruckmann, E.-M.I., B.V. Martemyanov, Bo Zhang

  Phys. Rev. D81:074501 (2010) [arXiv: 0912.4186 [hep-th]]